Developing novel indoles as antitubercular agents and simulated-annealing based analysis of their binding with MmpL3

Rajdeep Ray[1], Stutee Das[1], Sumit Raosaheb Birangal[1], Helena I. Boshoff[2], Jose Santinni Roma[2], Manisha Lobo[1], Raghu Chandrashekhar Hariharapura[3], G. Gautham Shenoy[*1]

[1]*Department of Pharmaceutical Chemistry, Manipal College of Pharmaceutical Sciences, Manipal Academy of Higher Education, Manipal, Karnataka-576104, India*

[2]*Tuberculosis Research Section, Laboratory of Clinical Immunology and Microbiology, National Institute of Allergy and Infectious Diseases, National Institutes of Health, Bethesda, MD 20892, USA*

[3]*Department of Pharmaceutical Biotechnology, Manipal College of Pharmaceutical Sciences, Manipal Academy of Higher Education, Manipal, Karnataka-576104, India*

[*]Corresponding author

E-mail: gautham.gs@manipal.edu, gauthamgs@rediffmail.com

Abstract

Aim:

This research aimed to develop novel indole-2-carboxamides as antitubercular agents through rational drug designing and understand their binding interactions.

Materials and Methods:

Novel indole-2-carboximides targeting MmpL3 were designed based on SAR, synthesized, and tested for their antitubercular and *iniBAC* induction properties. Classical docking and simulated annealing were utilised to understand protein-ligand binding.

Results:

Out of the 12 synthesized compounds, 5c, 5f, and 5i, were active against H37Rv and different MDR and XDR strains of *M. tuberculosis*. *iniBAC* promoter induction study indicated that those were inhibitors of MmpL3. Through the docking and simulated annealing studies, we identified the significant interactions at the MmpL3 binding site.

Conclusion:

We developed three potent antitubercular molecules that supposedly act via inhibiting MmpL3. Results from the molecular modelling studies can be utilised in future drug designing.

Keywords: MmpL3, indole-2-carboxamides, tuberculosis, molecular docking, simulated annealing;

1. Introduction

Tuberculosis (TB)is an infectious disease caused by the pathogenic bacterium *M. tuberculosis* that primarily affects the lungs. It is the 13th leading cause of death, globally. According to WHO global tuberculosis report 2023, an estimated 10.6 million people developed TB in 2022 worldwide. Out of 1.30 million deaths that reported due to TB, 665000 people were adult men, 423000 adult women, and 214000 were children. The estimated number of multidrug-resistant TB or rifampicin (MDR TB) cases was 410000 in 2022 with an estimated 160000 deaths globally [1].

According to the latest guidelines from WHO, a six-month regimen of isoniazid, rifampicin, ethambutol, and pyrazinamide should be used to treat drug-sensitive TB. This includes all four drugs to be administered for two months followed by isoniazid and rifampicin for the remaining four months [2]. Treatment of drug-resistant TB is more complex and requires the use of drugs that cause more adverse effects. Although the treatment success rate of rifampicin-resistant TB (RR-TB) has reached 60% in recent years, the treatment of multidrug-resistant (MDR) and extensively drug-resistant TB (XDR-TB) is very complicated with poor prognosis [1].

In spite of significant progress in the field of new drug discovery over the last few years, only three new antitubercular drugs have been approved in the last 50 years viz. bedaquiline, delamanid, and pretomanid. Moreover, all the three drugs have been approved in the last decade [3,4]. As of 2022, there are ten antitubercular candidates in Phase 2 clinical trials viz. delpazolid, sutezolid, sudapyridine (WX-081), BTZ-043, TBA-7371, OPC-167832, GSK-656, SQ-109, telacebec, and SPR720. The molecules other than delpazolid, sutezolid, and sudapyridine, are from new chemical classes. Surprisingly, currently there are no new antitubercular candidates in Phase 3 clinical trials [4]. The lengths of the existing anti-tubercular therapy regimens, adverse effects, emergence of drug resistance, patient non-compliance, and the fact that very few molecules have been approved in the last few years for the treatment of tuberculosis, justify the need for the discovery and development of more efficacious, and safer drugs which can simplify the current therapeutic regimen.

MmpL (Mycobacterial membrane protein Large) proteins have been reported to be vital for the formation of mycobacterial cell envelope [5]. These proteins belong to the RND (Resistant Nodulation and Divison) superfamily, and act by the proton motive force. Till now, 13 MmpL proteins have been identified in *M. tuberculosis* [6]. MmpL8 has been

reported to be associated with fatty acid synthesis whereas MmpL10 acts by transporting 2,3-diacyltrehaloses (DAT) and penta-acyltrehaloses (PAT). MmpL11, on the other hand, is reported to induce the transport of monomer-mycolyl diacylglycero and mycolate wax ester [7]. Among others, MmpL7 is known to act by transport of phthiocerol dimycocerosate while MmpL4 and MmpL5 are vital for the siderophore-mediated iron acquisition and have roles in siderophore export [8,9]. Distinctly, MmpL5 and MmpL7 are also associated with drug efflux [10]. MmpL3 plays an essential role through the transport of trehalose monomycolate required for cell wall biogenesis in mycobacteria making it a particularly attractive antitubercular target [11]. Mycolic acids are the essential components of the cell envelop of *M. tuberculosis.* These are synthesized by three enzymatic units viz. fatty acid synthase I, fatty acid synthase II and polyketide synthase, and act as components of trehalose monomycolate (TMM) and trehalose dimycolate (TDM). These are also covalently linked to mycolyl-arabinogalactan-peptidoglycan (mAGP) [12,13]. The trehalose monomycolate transported by MmpL3 to the periplasmic region serves as the precursor for the synthesis of trehalose dimycolate as well as the mycolates in mAGP through the enzymatic activity of the Ag85 complex [12]. Multiple inhibitors of MmpL3 have been identified over the past few years that were seen to inhibit mycolic acid synthesis by targeting MmpL3 [14]. These compounds were initially identified through phenotypic assays and subsequent studies have shown them to reduce TDM and mycolyl-arabinogalactan synthesis and increase TMM concentration [15]. Gene knockout models of MmpL3 have also resulted in mycobacterial death for both invitro and invivo study models, thus validating its role as a drug target [16-18]. Some of the earlier MmpL3 inhibitors like SQ109, AU1235, BM212, etc., and many newly identified molecules, present a diverse group of scaffolds [19]. This phenomenon has made MmpL3 a very promising protein target to explore.

Multiple studies have shown indole-2-carboxamides and pyrrole-2-carboxamides as potent antitubercular molecules that acts via inhibiting MmpL3 [20-23]. Onajole et al. (2013), reported the structure-antitb activity relationship (SAR), of indole-2-carboxamides [20]. Lun et al. (2013) also reported that these molecules were potent against drug resistant TB and in vivo [24]. Moreover, mutations induced by the indole-2-carboxamides on Mmpl3 confirmed the target. Jiricek et al. also reported novel indole-2-caroboxamides with very high potency against *M. Tuberculosis* [23]. More recently, Bhattarai et al. (2023), designed and reported acetamide-based compounds based on the indole-2-carboxamide pharmacophore. The compounds were potent and had better ADME profile than its indole analogue [25].

Previously, we have reported a series of novel antitubercular compounds which were proposed to act through inhibition of the MmpL3 protein. In this study, we describe the design and evaluation of new indole-2-carboxamides as an improvement on our previous series. These had indole-2-carboxamide as the core moiety and some of the molecules had shown promising activity [26]. In the previous study, we had computationally designed the molecules based on in silico prediction of their binding to MmpL3 by using homology models, performing molecular docking and molecular dynamics, and calculating the free energies for binding [27]. The publication of the MmpL3 protein structure of *M. Tuberculosis* (PDB ID - 7NVH) provided us with the opportunity to use it for structure-guided design in this work [28]. The in-silico screening of our designed molecules was based on a model built on the MmpL3 structures of PDB ID 7NVH as well as the 6AJI structure. We additionally utilised the technique of simulated annealing to analyse the binding interaction pattern of the designed indole-2-carboxamides inside the MmpL3 binding pocket. The indole-2-carboxamides were synthesized and confirmed to have antitubercular activity against drug sensitive as well as a panel of drug-resistant clinical strains of the pathogen. Support for their on-target activity was confirmed by reporter strains that flag inhibitors of cell wall biogenesis.

2. Materials and Methods

2.1 Software and tools

The structures and reaction schemes were drawn using Marvin Sketch 22.15. The computational tasks were performed using Maestro 12.7.156 (Release 2021-1 of Schrodinger).

2.2 Design of new molecules

In our previous work, we had explored the third position of indole-2-carboxamides with various substitutions. Molecules 3a, 3b and 5b were found to be the most potent molecules with respective MIC values (in 1-week BSA free medium) of 3.13 µM, 1.56 µM, 6.25 µM, and 3.13 µM against H37Rv strain of *M. tuberculosis* [22]. It was deduced that methyl group substitution or introduction of methylene attached benzyl amino group at the 3rd position clearly helped the molecules to become active provided that there was a 4-CH_3 substitution on the cyclohexyl group. Using these findings, in the present study, we attempted expanding the alkyl chain at the third position of indole-2-carboxaxmides (Fig. 1A). In another set of designed molecules, 4-Cl phenylamino group was attached to the indole-2-carboaximdes with

a methylene linker. Similarly, a 4-Cl benzylamino group and a 4-CH_3 benzylamino group were attached to the indole-2-carboaximdes with a methylene linker (Fig. 1B). All the designed molecules were then analyzed by docking them and confirming the presence of desired interactions at the MmpL3 binding pocket. MMBGSA study was also performed with these molecules and those that crossed (less than) cut-off scores of -40 kcal/mol (dG bind) and -8 (docking) were considered for synthesis. We initially used the protein model from our previous work for the screening of our molecules [27]. The molecules were synthesized thereafter. But as a new MmpL3 structure was published, we developed a new model (further discussed in the next section). The molecules were redocked, revalidated, and we made sure they crossed the cut-off scores with the new model. In this paper we have only discussed the modelling results from the new model as it was more reliable.

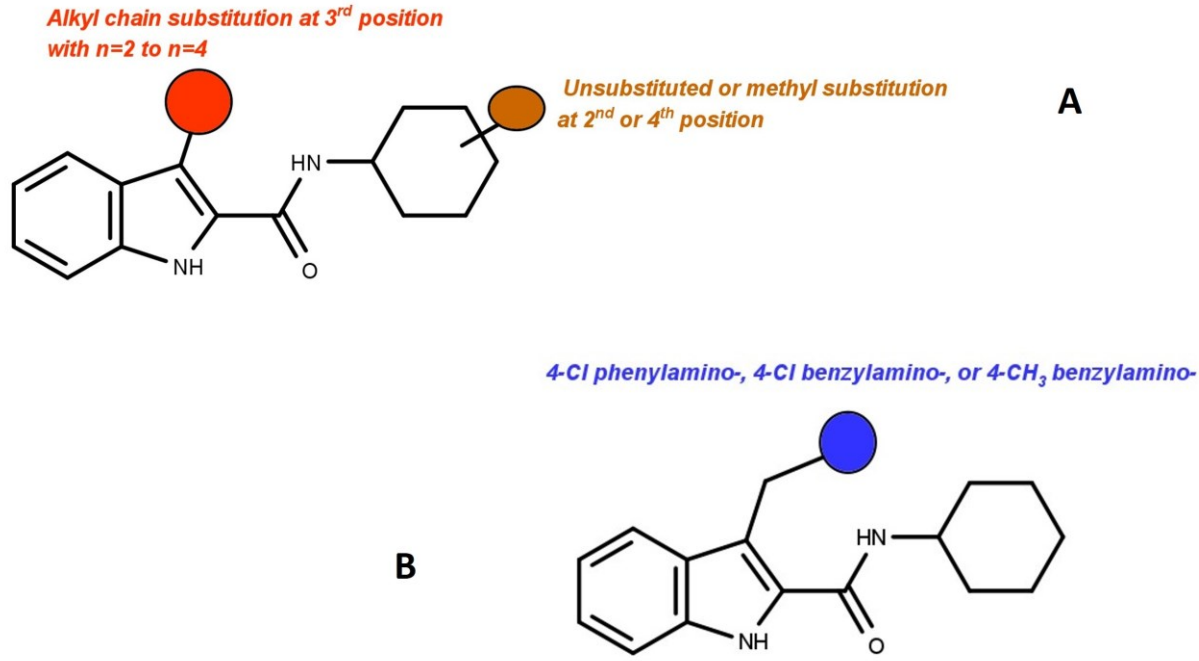

Fig. 1 Two different design strategy of new molecules shown in (A) and (B) where n refers to the number of carbons in the alkyl chain

2.3 Homology modelling

In this work, we have used the PDB IDs 7NVH and 6AJI as templates for modelling. 6AJI is a *M. smegmatis* MmpL3 structure bound to rimonabant. This was primarily selected because the bound ligand resembled the shape of our designed molecules. 7NVH is the first *M. tuberculosis* MmpL3 structure to be published. It is a cryo-EM structure which contained the trans-membrane and the periplasmic part of the protein [28]. Sitemap was initially used to

identify the relevant binding sites but on docking with several MmpL3 inhibitors, inconsistent results were obtained. In the trans-membrane region, it could generate only one site (S1), but it was at a distant location from the actual binding site acquired from the crystal structure. Moreover, it was unlikely that the pocket created due to huge expansion upon actual ligand binding (as shown by Zhang et al. with *M. smegmatis*' ligand bound MmpL3 structures, e.g., 6AJI, 6AJJ etc.) could be modelled from the Sitemap structures. Thus, in this case, we used the chimera mode of modelling in Prime where the binding pocket structure was being modelled from 6AJI and 7NVH was used for modelling the remaining protein. The missing loop regions were capped to prevent unwanted deviations during simulations since it was not in the vicinity of the binding site.

2.4 Molecular Dynamics

2.4.1 Model Validation

Classical molecular dynamics was used to validate the model. The system was built using the System Setup tool from Desmond (Maestro). We used single-point charge (SPC) as the explicit water model and a phosphatidylcholine (POPC) membrane was built encompassing the residues 14–34, 186–206, 210–230, 236–256, 287–307, 315–335, 397–417, 563–583, 587–607, 617–637, 673–693, and 699–719. 8 chloride anions were subsequently added to neutralize the system. OPLS4 was the force field of choice for the subsequent simulations. Post minimization, the system was relaxed using a special in-built relaxation protocol (Maestro) for membrane proteins. It included additional restraints to prevent entry of water molecules into the membrane-protein gaps during the equilibration process. The NPγT ensemble (pressure = 1.013 bar, surface tension = 4000 bar-Å, temperature = 300 K, with constant number of particles) was chosen for the production run and Noose-Hover and Martyna–Tobias–Klein were the chosen thermostat and barostat methods, respectively. Timestep of 2 femtoseconds (fs) were used to run the simulation [27].

2.4.2 Simulated annealing

For analysing the protein-ligand binding in a robust manner, we utilised the simulated annealing (SA) method instead of classical MD simulation. It involves controlled heating and cooling of the system to reach a lower energy space than conventional MD. The timesteps for this workflow were divided as 30 ps (10 K), 100 ps (100 K), 200 ps (300 K), 300 ps (400 K), 500 ps (400 K), and 1000 ps (300 K) [29]. It is assumed that rising the temperature beyond 300 K and again cooling it helps to attain regions closer to the global minima in systems. In

order to ensure that the protein secondary and tertiary structures are not disturbed due to the high temperature attained, we compared the MD data for classical and simulated annealing. Both classical MD and simulated annealing was run for 5fT-MmpL3 complex and the results were analysed. It was concluded that SA did not result in any structural disintegration of the protein. Moreover, the potential energy of the complex was significantly lower for SA simulation (discussed elaborately in section 3.1). Thus, SA was chosen for the simulation of the remaining complexes for this study i.e., 5cC-MmpL3, 5cT-MmpL3, 5iC-MmpL3, and 5iT-MmpL3. Further, MMGBSA was performed on the post-MD frames from each of the simulated complex. The frames were considered from the time simulations had equilibrated.

[a]Scheme 1

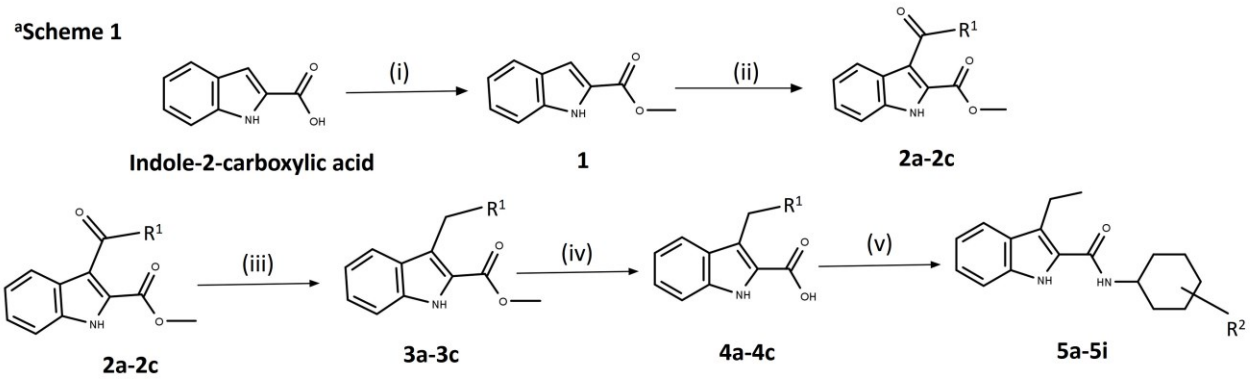

5a: $R^1 = CH_3$, R^2 = H; 5b: $R^1 = CH_3$, R^2 = 2-CH_3; 5c: $R^1 = CH_3$, R^2 = 4-CH_3; 5d: $R^1 = C_2H_5$, R^2 = H; 5e: $R^1 = C_2H_5$, R^2 = 2-CH_3; 5f: $R^1 = C_2H_5$, R^2 = 4-CH_3; 5g: $R^1 = C_3H_7$, R^2 = H; 5h: $R^1 = C_3H_7$, R^2 = 2-CH_3; 5i: $R^1 = C_3H_7$, R^2 = 4-CH_3;

[a]Reagents and conditions: (i) H_2SO_4, MeOH, reflux, 24 hours; (ii) $AlCl_3$, acyl chloride, DCM, 0°C-50°C, 2-3 hours; (iii) triethylsilane, CF_3COOH, 0°C-R.T, 10-12 hours; (iv) KOH, Water, 90^0C, 1 hour; (v) EDC·HCl, HOBt, DCM, TEA, corresponding cyclohexylamines, R.T., 16-20 hours.

H_2SO_4: Sulphuric acid, MeOH: Methanol, $AlCl_3$: Aluminium trichloride, DCM: Dichloromethane, CF_3COOH: Trifluroacetic acid, KOH: Potassium hydroxide, EDC·HCl: (3-Dimethylamino-propyl)-ethyl-carbodiimide hydrochloride, HOBt: Hydroxybenzotriazole, DCM: Dichloromethane, TEA: Triethylamine, R.T.: Room temperature.

2.5 Synthesis

Synthesis of methyl1H-indole-2-carboxylate (1)

Indole-2-carboxylic acid (25 mmol) was dissolved in methanol (MeOH) (50 mL). It was followed by the addition of sulphuric acid (H_2SO_4) (37.2 mmol) and the mixture was refluxed for 24 hours. The reaction solvent was distilled under vacuum upon completion of the reaction followed by addition of ethyl acetate (EtOAc) (20 mL) to the mixture. A saturated solution of sodium carbonate was added slowly under cold condition to the mixture and the pH was brought to 8. EtOAc (3 × 50 mL) wash was given to extract the aqueous layer. The

organic layer was dried over sodium sulphate and then distilled under vacuum to give ethyl indole-2-carboxylate [31].

Synthesis of methyl 3-acetyl-1H-indole-2-carboxylate (2a)

1 (17 mmol) was dissolved in anhydrous dichloromethane (DCM) (75 mL) and anhydrous aluminium chloride (17 mmol) powder was added to the solution followed by the dropwise addition of the acetyl chloride (20.5 mmol) at room temperature. The reaction mixture was refluxed with stirring under nitrogen atmosphere for 2−3 hours. Upon completion of reaction, the mixture was poured into ice-cold water (H_2O) (150 mL), then treated with saturated sodium carbonate (Na_2CO_3) solution till pH reached 8. EtOAc (3 × 50 mL) was then used to extract the solution. Successive washing of the combined organic layer was carried out with H_2O (30 mL) and brine solution (30 mL). The organic layer was separated and dried over anhydrous sodium sulphate. Finally, distillation of the solvent was done under vacuum to yield the crude product [32].

Synthesis of methyl 3-propanoyl-1H-indole-2-carboxylate (2b), methyl 3-propanoyl-1H-indole-2-carboxylate (2c)

The general method for the synthesis of 2a was followed with the corresponding acyl chlorides [32].

Synthesis of methyl 3-ethyl-1H-indole-2-carboxylate (3a)

Triethylsilane (20 mmol) was added dropwise to the solution of 2 (10 mmol) in trifluoracetic acid (CF_3COOH) (20 mmol) at 0°C. The reaction mixture was then stirred at room temperature and the stirring was continued for 10−12 hours. Upon completion of the reaction, the mixture was poured onto ice and treated with saturated aqueous solution of sodium carbonate. The pH was adjusted to 7 followed by extraction with EtOAc (2 × 50 mL). The combined organic phase was washed with H_2O (30 mL) and brine solution (30 mL) and dried over anhydrous sodium sulphate (Na_2SO_4). The solvent was then distilled under vacuum to yield the crude product [33].

Synthesis of methyl 3-propyl-1H-indole-2-carboxylate (3b), 3-butyl-1H-indole-2-carboxylate (3c)

The general method for the synthesis of 3a was followed [33].

Synthesis of 3-ethyl-1H-indole-2-carboxylic acid (4a)

3 (8 mmol) was added to an aqueous solution (20 mL) of potassium hydroxide (KOH) (16 mmol) and heated to 90 °C. The reaction was continued for 1 hour. After completion of reaction, the reaction mixture was allowed to cool to room temperature and the pH was adjusted to 3-4 by the careful addition of 6N HCl. The solid was then filtered and dried at 60°C for 48 hours [33].

Synthesis of 3-propyl-1H-indole-2-carboxylic acid (4b), 3-butyl-1H-indole-2-carboxylic acid (4c)

The general method for the synthesis of 4a was followed [33].

Synthesis of N-cyclohexyl-3-ethyl-1H-indole-2-carboxamide (5a)

1-(3-Dimethylaminopropyl)-3-ethylcarbodiimide hydrochloride (EDC·HCl) (4.4 mmol) and Hydroxybenzotriazole (HOBt) (4.4 mmol) were added to the mixture of 4 and DCM (20 mL) at room temperature. It was stirred for 10 minutes followed by the addition of either N,N-diisopropylethylamine (DIPEA) (5.5 mmol) or triethylamine (TEA) (5.5 mmol) and cyclohexylamine (5.5 mmol). On completion of the reaction, the solvent was distilled off under vacuum and a sticky mass was left over. Dimethylformamide (DMF) (3 mL) and water (10 mL) was added to it and stirred for 10 mins. The crude compound was obtained upon filtration. It was washed with methanol (stirring for 30 minutes) and subsequently filtered to yield the pure solid compound. The solid was then dried at 60^0 C for 48 hours [34,35].

Synthesis of 3-ethyl-N-(2-methylcyclohexyl)-1H-indole-2-carboxamide (5b),
3-ethyl-N-(4-methylcyclohexyl)-1H-indole-2-carboxamide (5c),
N-cyclohexyl-3-propyl-1H-indole-2-carboxamide (5d),
N-(2-methylcyclohexyl)-3-propyl-1H-indole-2-carboxamide (5e),
N-(4-methylcyclohexyl)-3-propyl-1H-indole-2-carboxamide (5f),
3-butyl-N-cyclohexyl-1H-indole-2-carboxamide (5g),
3-butyl-N-(2-methylcyclohexyl)-1H-indole-2-carboxamide (5h),
3-butyl-N-(2-methylcyclohexyl)-1H-indole-2-carboxamide (5i)

The general method for the synthesis of 5a was followed with corresponding indole-2-carboxylic acids and their corresponding cyclohexylamines [34,35].

N-cyclohexyl-3-ethyl-1H-indole-2-carboxamide (5a)

Yield 70% (White Powder). ^{1}H NMR (400 MHz, $CDCl_3$) δ 8.97 (s, 1H, indole N-H), 7.63 (d, J = 8 Hz, 1H, aromatic H), 7.38 (d, J = 8 Hz, 1H, aromatic H), 7.28 (t, J = 7 Hz, 1H, aromatic H), 7.13 (t, J = 7.6 Hz, 1H, aromatic H), 5.96 (d, J = 6.8 Hz, 1H, amide N-H), 4.08–4.06 (m, 1H, N attached C-H), 3.00 (q, J = 7.6 Hz, 3H, aliphatic C-H), 2.07–2.04 (m, 2H, aliphatic C-H), 1.77–1.74 (m, 2H, aliphatic C-H), 1.67–1.64 (m, 1H, aliphatic C-H), 1.53–1.44 (m, 2H, aliphatic C-H), 1.37-1.2 (m, 6H, aliphatic C-H); ^{13}C NMR (DMSO-d_6) δ 161.31, 135.69, 127.56, 127.33, 124.00, 121.69,120.02, 119.48, 112.29, 48.30, 32.96, 25.74, 25.19, 17.74, 16.09; MS (ESI) m/z calcd for $C_{17}H_{22}N_2O$ ($[M-H]^-$) 269.38; found 269.29.

3-ethyl-N-(2-methylcyclohexyl)-1H-indole-2-carboxamide (5b)

Yield 65% (White Powder). ^{1}H NMR (400 MHz, $CDCl_3$) δ 8.91 (s, 1H, indole N-H), 7.64 (d, J = 8 Hz, 1H, aromatic H), 7.39 (d, J = 8 Hz, 1H, aromatic H), 7.28 (t, J = 7.4 Hz, 1H, aromatic H), 7.14 (t, J = 7.6 Hz, 1H, aromatic H), 5.96 (d, J = 8.4 Hz, 1H, amide N-H), 3.78 – 3.75 (m, 1H, N attached C-H), 3.01 (q, J = 7.6 Hz, 3H, aliphatic C-H), 2.17 – 2.11 (m, 2H, aliphatic C-H), 1.84 – 1.71 (m, 2H, aliphatic C-H), 1.45 – 1.33 (m, 5H, aliphatic C-H), 1.30 – 1.17 (m, 3H, aliphatic C-H), 1.03 (d, J = 6.4 Hz, 3H, aliphatic C-H); ^{13}C NMR (DMSO-d_6) δ 161.70, 135.69, 127.57, 127.54,123.91, 121.86, 121.27, 119.98, 119.46, 112.29, 54.0, 37.68, 34.61, 33.52, 25.97, 25.76, 19.78, 17.75, 16.15; MS (ESI) m/z calcd for $C_{18}H_{24}N_2O$ ($[M-H]^-$) 283.4; found 283.27.

3-ethyl-N-(4-methylcyclohexyl)-1H-indole-2-carboxamide (5c)

Yield 68% (White Powder). ^{1}H NMR (400 MHz, $CDCl_3$) δ 8.96&8.93 (2s, 1H, indole N-H), 7.57 (t, J = 8 Hz, 1H, aromatic H), 7.19 (br d, J = 8 Hz, 1H, aromatic H), 7.23 - 7.19 (m, 1H, aromatic H), 7.08 (br d, J = 8 Hz, 1H, aromatic H), 6.20-5.79 (2s, 1H, amide N-H), 4.29-3.89 (2m, 1H, N attached C-H), 2.98-2.91 (m, 2H, aliphatic C-H), 2.08-2.05 (br d, 1H, aliphatic C-H), 1.78 - 1.64 (m, 4H, aliphatic C-H), 1.33 - 1.08 (m, 7H, aliphatic C-H), 0.90&0.87 (2d, J = 6 Hz & 5.8 Hz, 3H, aliphatic C-H); ^{13}C NMR (DMSO-d_6) δ 161.61, 161.39, 135.71, 135.67, 127.57, 127.36, 127.33, 124.02, 121.68, 121.60, 120.02, 119.49, 112.30, 48.45, 45.93, 34.14, 32.83, 32.04, 30.11, 29.04, 22.68, 21.16, 17.83, 17.71, 16.14, 16.10; MS (ESI) m/z calcd for $C_{18}H_{24}N_2O$ ($[M-H]^-$) 283.4; found 283.25.

N-cyclohexyl-3-propyl-1H-indole-2-carboxamide (5d)

Yield 80% (White Powder). ^{1}H NMR (400 MHz, $CDCl_3$) δ 8.99 (s, 1H, indole N-H), 7.63 (d, J = 8 Hz, 1H, aromatic C-H), 7.38 (d, J = 8 Hz, 1H, aromatic C-H), 7.27 (br t, 1H, aromatic C-H), 7.12 (t, J = 7.4 Hz, 1H, aromatic C-H), 5.99 (d, J = 6.8 Hz, 1H, amide N-H), 4.07–4.05 (m, 1H, N attached C-H), 2.95 (t, J = 7.6 Hz, 2H, aliphatic C-H), 2.06 (br d, 2H, aliphatic C-H), 1.79–1.73 (m, 4H, aliphatic C-H), 1.67–1.63 (m, 1H, aliphatic C-H), 1.53–1.43 (m, 2H, aliphatic C-H), 1.36–1.27 (m, 3H, aliphatic C-H), 1.05 (t, 3H, aliphatic C-H); ^{13}C NMR (DMSO-d_6) δ 161.39, 135.63, 128.09, 127.86, 123.91, 120.14, 119.79, 119.46, 112.25, 48.29, 32.94, 26.38, 25.74, 25.19, 24.30, 14.50; MS (ESI) m/z calcd for $C_{18}H_{24}N_2O$ ([M-H]$^-$) 283.4; found 283.30.

N-(2-methylcyclohexyl)-3-propyl-1H-indole-2-carboxamide (5e)

Yield 75% (White Powder). ^{1}H NMR (400 MHz, $CDCl_3$) δ 9.04 (s, 1H, indole N-H), 7.56 (d, J = 8 Hz, 1H, aromatic C-H), 7.32 (d, J = 8 Hz, 1H, aromatic C-H), 7.21 (br t,1H, aromatic C-H), 7.05 (t, J = 8 Hz, 1H, aromatic C-H), 5.81 (s, 1H, amide N-H), 3.72-3.67 (m, 1H, N attached C-H), 2.89 (t, J = 8 Hz, 2H, aliphatic C-H), 2.06 (br d,1H, aliphatic C-H), 1.77–1.64 (m, 6H, aliphatic C-H), 1.40–1.18 (m, 2H, aliphatic C-H), 1.18–1.15 (m, 3H, aliphatic C-H), 0.99-0.89 (m, 5H, aliphatic C-H); ^{13}C NMR (DMSO-d_6) δ 161.79, 135.62, 128.11, 128.08, 123.82, 120.12, 119.44, 119.34, 112.25, 54.00, 37.64, 34.62, 33.51, 26.40, 25.96, 25.76, 24.38, 19.77, 14.48; MS (ESI) m/z calcd for $C_{19}H_{26}N_2O$ ([M-H]$^-$) 297.43; found 297.27.

N-(4-methylcyclohexyl)-3-propyl-1H-indole-2-carboxamide (5f)

Yield 76% (White Powder). ^{1}H NMR (400 MHz, $CDCl_3$) δ 9.00&8.96 (2s, 1H, indole N-H), 7.63 (br d, 1H, aromatic C-H), 7.38 (d, J = 8 Hz, 1H, aromatic C-H), 7.28 (br t, 1H, aromatic C-H), 7.15–7.10 (m, 1H, aromatic C-H), 6.28&5.58 (2d, 1H, amide N-H), 4.36&3.95 (2m, 1H, N attached C-H), 3.00–2.92 (m, 2H, aliphatic C-H), 2.13 (br d, 1H, aliphatic C-H), 1.87–1.68 (m, 8H, aliphatic C-H), 1.54–1.01 (m, 7H, aliphatic C-H), 0.97&.93 (2d, J = 6.8 Hz & 6.4 Hz, 3H, 4-CH_3 at cyclohexyl); ^{13}C NMR (DMSO-d_6) δ 161.72, 161.46, 135.65, 135.61, 128.08, 127.93, 127.86, 123.92, 120.15, 119.80, 119.57, 119.47, 112.27, 112.24, 48.45, 45.90, 34.14, 32.82, 32.04, 30.12, 29.04, 26.56, 26.35, 24.37, 24.28, 22.68, 21.21, 14.55, 14.50; MS (ESI) m/z calcd for $C_{19}H_{26}N_2O$ ([M-H]$^-$) 297.43; found 297.23.

3-butyl-N-cyclohexyl-1H-indole-2-carboxamide (5g)

Yield 72% (White Powder). ^{1}H NMR (400 MHz, DMSO-*d*$_6$) δ 11.11 (1s, 1H, indole N-H), 7.69 (d, J = 7 Hz, 1H, amide N-H), 7.59 (d, J = 8 Hz, 1H, aromatic C-H), 7.38 (d, J = 8 Hz, 1H, aromatic C-H), 7.19 (t, J = 7.2 Hz, 1H, aromatic C-H), 7.02 (t, J = 8 Hz, 1H, aromatic C-H), 3.80-3.77 (m, 1H, N attached C-H), 3.02 (t, J = 7.2 Hz, 2H, aliphatic C-H), 1.90–1.53 (m, 7H, aliphatic C-H), 1.32–1.19 (m, 7H, aliphatic C-H), 0.88 (t, J = 7.2 Hz, 3H, aliphatic C-H); ^{13}C NMR (DMSO-*d*$_6$) δ 161.40, 135.64, 128.00, 127.79, 123.91, 120.11, 119.94, 119.45, 112.26, 48.29, 33.35, 32.95, 25.74, 25.19, 24.08, 22.66, 14.37; MS (ESI) m/z calcd for $C_{19}H_{26}N_2O$ ([M-H]$^-$) 297.43; found 297.29.

3-butyl-N-(2-methylcyclohexyl)-1H-indole-2-carboxamide (5h)

Yield 72% (White Powder). ^{1}H NMR (400 MHz, DMSO-*d6*) δ 11.27&11.07 (2s, 1H, indole N-H), 7.65–7.60 (2d, 2H, aromatic C-H, amide N-H), 7.40–7.36 (m, 1H, aromatic C-H), 7.40-7.36 (m, 1H, aromatic C-H), 7.18 (t, J = 7.4 Hz, 1H, aromatic C-H), 7.02 (t, J = 7.8 Hz, 1H, aromatic C-H), 4.14–3.58 (2m, 1H, N attached C-H), 3.02 (t, J = 7.2 Hz, 2H, aliphatic C-H attached to 3rd position of indole ring), 1.87–1.64 (m, 4H, aliphatic C-H), 1.56–1.44 (m, 4H, aliphatic C-H), 1.35-1.2 (m, 5H, aliphatic C-H), 0.93–0.86 (m, 6H, aliphatic C-H); ^{13}C NMR (DMSO-*d*$_6$) δ 161.79, 135.68, 135.64, 128.01, 127.60, 123.98, 123.82, 120.08, 119.53, 119.49, 119.43, 112.27, 53.99, 49.59, 37.65, 34.61, 33.52, 33.46, 30.13, 29.46, 25.97, 25.76, 24.33, 24.11, 22.74, 22.67, 19.76, 14.38; MS (ESI) m/z calcd for $C_{20}H_{28}N_2O$ ([M-H]$^-$) 311.46; found 311.31.

3-butyl-N-(4-methylcyclohexyl)-1H-indole-2-carboxamide (5i)

Yield 71% (White Powder). ^{1}H NMR (400 MHz, $CDCl_3$) δ 9.01&8.99 (2s, 1H, indole N-H), 7.57-7.54 (m, 1H, aromatic C-H), 7.32-7.30 (m, 1H, aromatic C-H), 7.23-7.20 (m, 1H, aromatic C-H), 7.08-7.05 (m, 1H, aromatic C-H), 6.23&5.86 (2s, 1H, amide N-H), 4.30-3.86 (2m, 1H, N attached C-H), 2.95-2.87 (2t, J = 8 Hz, 2H, aliphatic C-H), 2.06 (br d, 1H, aliphatic C-H), 1.80-1.61 (m, 5H, aliphatic C-H), 1.46-1.36 (m, 3H, aliphatic C-H), 1.22-1.02 (m, 3H, aliphatic C-H), 0.94-0.68 (m, 7H, aliphatic C-H); ^{13}C NMR (DMSO-*d*$_6$) δ 161.73, 161.47, 135.67, 135.63, 128.02, 128.00, 127.86, 127.78, 123.91, 120.11, 119.96, 119.71, 119.46, 112.41, 48.45, 45.90, 34.14, 33.45, 33.34, 32.83, 32.04, 30.11, 29.05, 24.27, 24.06, 22.74, 22.68, 22.65, 21.16, 14.37; MS (ESI) m/z calcd for $C_{20}H_{28}N_2O$ ([M-H]$^-$) 311.46; found 311.24.

[a]Scheme 2

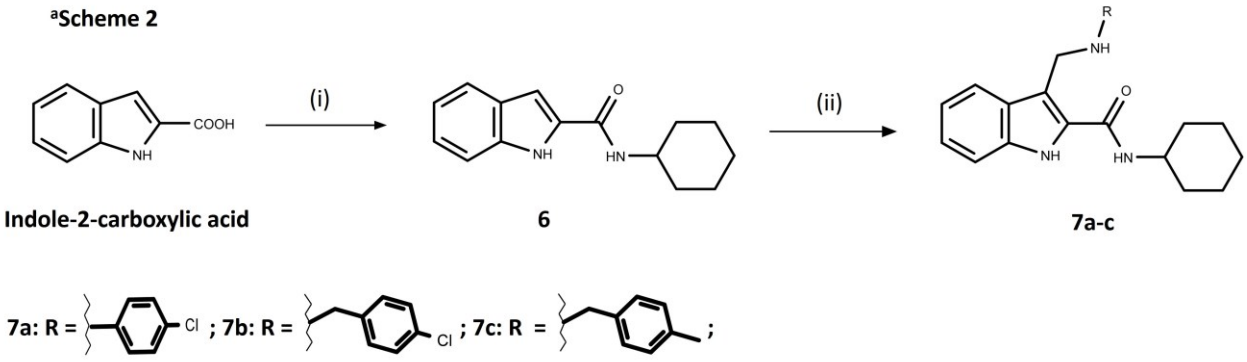

[a]Reagents and conditions: (i) EDC·HCl, HOBt, DCM, TEA, corresponding cyclohexylamines, R.T., 16-20 hours; (ii) substituted amines, formaldehyde, indole-2-carboxamide, acetic acid, R.T., 1-2 hours.

EDC·HCl: (3-Dimethylamino-propyl)-ethyl-carbodiimide hydrochloride, HOBt: Hydroxybenzotriazole, DCM: Dichloromethane, TEA: Triethylamine, R.T.: Room temperature.

Synthesis of N-cyclohexyl-1H-indole-2-carboxamide (6)

The general method for the synthesis of 5a was followed with indole-2-carboxylic acid and unsubstituted cyclohexylamine. The product was carried over to the next step after giving DMF/H_2O (3 mL/10 mL) wash [34,35].

Synthesis of 3-({[(4-chlorophenyl)methyl]amino}methyl)-N-cyclohexyl-1H-indole-2-carboxamide (7a)

4-Chloroaniline (4.8 mmol) and formaldehyde (4 mmol) were added to CH_3COOH (5 mL) and the solution was stirred for 30 minutes at room temperature. To the reaction mixture, 6 (4 mmol) was added, and the stirring was continued for an hour. The completion of the reaction was confirmed by TLC. 20% sodium carbonate was then added to the mixture and the pH was adjusted to 8-9. The crude compound was filtered and washed with H_2O to remove the excess base. It was then stirred in MeOH for 30 minutes to give a pure product [36-38].

Synthesis of 3-{[(4-chlorophenyl)amino]methyl}-N-cyclohexyl-1H-indole-2-carboxamide (7b), N-cyclohexyl-3-({[(4-methylphenyl)methyl]amino}methyl)-1H-indole-2-carboxamide (7c)

The general method for the synthesis of 7a was followed with corresponding benzylamines. Purification was done by dissolving the crude solid in DCM followed by addition of oxalic acid (4.8 mmol). The mixture was stirred for 3 hours. Resulting oxalate salt of the compound was then filtered followed by basification with sodium carbonate solution. The free base was

then extracted with EtOAc or DCM (3 x 10 mL) and the solvent was distilled under vacuum to give the pure compounds [36-38].

3-{[(4-chlorophenyl)amino]methyl}-N-cyclohexyl-1H-indole-2-carboxamide (7a)

Yield 82% (Pale yellow powder). ^{1}H NMR (400 MHz, DMSO-d_6) δ 11.5 (s, 1H, indole N-H), 8.31 (d, J = 7.6 Hz, 1H, amide N-H), 7.77 (d, J = 8.0 Hz, 1H, aromatic H), 7.42 (d, J = 8.4 Hz, 1H, aromatic H), 7.2 (t, J = 7.6 Hz, 1H, aromatic H), 7.12 (d, J = 8.4 Hz, 2H, aromatic H), 7.05 (t, J = 7.6 Hz, 1H, aromatic H) 6.78 (d, J = 8.4 Hz, 2H, aromatic H), 6.26 (t, J = 5.2 Hz, 1H, aromatic), 4.54 (d, J = 5.2 Hz, 2H, N-CH_2 attached to 3rd position of indole ring), 3.81-3.79 (m, 1H, cyclohexyl N-C-H), 1.82 (br d, 2H, aliphatic C-H), 1.64-1.50 (m, 3H, aliphatic C-H), 1.34-1.25 (m, 2H, aliphatic C-H), 1.18-1.05 (m, 3H, aliphatic C-H); ^{13}C NMR (DMSO-d_6) δ 161.09, 147.89, 135.55, 130.09, 128.98, 127.78, 124.02, 120.75, 120.39, 119.98, 115.13, 114.21, 112.56, 47.92, 38.16, 32.80, 25.67, 24.60; MS (ESI) m/z calcd for $C_{22}H_{24}ClN_3O$ ([M-H]$^-$) 380.9; found 380.44.

3-({[(4-chlorophenyl)methyl]amino}methyl)-N-cyclohexyl-1H-indole-2-carboxamide (7b)

Yield 80% (White powder). ^{1}H NMR (400 MHz, $CDCl_3$) δ 10.27 (s, 1H, indole N-H), 9.77 (s, 1H, aliphatic secondary amine N-H), 7.48 (br d, 1H, aromatic H), 7.38 (br d, 1H, aromatic H), 7.25 (br d, 2H, aromatic H), 7.19-7.14 (s, 3H, aromatic H), 7.05 (br d, 1H, aromatic H), 4.06 (s, 2H, N-CH_2 attached to chlorobenzene), 3.95-3.93 (m, 1H, cyclohexyl N-C-H), 3.73 (s, 2H, N-CH_2 attached to 3rd position of indole ring), 1.95 (d, J = 8.0 Hz, 3H), 1.67 (d, J = 8.0 Hz, 1H), 1.36 (br d, 3H), 1.15 (br d, 4H); ^{13}C NMR ($CDCl_3$) δ 160.30, 136.45, 133.62, 132.14,129.92, 128.52, 127.69, 127.11, 122.93, 118.96, 118.01, 111.00, 110.93, 50.69, 47.48, 41.44, 32.28, 24.68, 23.92; MS (ESI) m/z calcd for $C_{23}H_{26}ClN_3O$ ([M+H]$^+$) 396.93; found 396.22.

N-cyclohexyl-3-({[(4-methylphenyl)methyl]amino}methyl)-1H-indole-2-carboxamide (7c)

Yield 75% (White powder). ^{1}H NMR (400 MHz, DMSO-d_6) δ 11.49 (s, 1H, indole N-H), 10.79 (d, J = 7.6 Hz, 1H, amide N-H), 7.54 (d, J = 8.0 Hz, 1H, aromatic H), 7.40 (d, J = 8.0 Hz, 1H, aromatic H), 7.21-7.12 (m, 5H, aromatic H), 7.02 (t, J = 7.4 Hz, 1H, aromatic H), 3.98 (s, 2H, N-CH_2 attached to chlorobenzene), 3.81-3.73 (m, 1H, cyclohexyl N-C-H), 3.66 (br d, 2H, N-CH_2 attached to 3rd position of indole ring), 2.29 (s, 3H, aliphatic C-H), 1.86-1.83 (m, 2H, aliphatic C-H), 1.68-1.54 (m, 3H, aliphatic C-H), 1.33-1.09 (m, 5H, aliphatic C-H); ^{13}C NMR (DMSO-d_6) δ 161.12, 137.07, 136.23, 135.26, 131.34, 129.15, 128.53, 128.30,

123.51, 119.65, 112.86, 112.61, 51.66, 48.08, 42.22, 33.04, 25.71, 24.95, 21.16; MS (ESI) m/z calcd for $C_{24}H_{29}N_3O$ ($[M+H]^+$) 376.52; found 376.24.

2.6 Antitubercular Studies on *M. tuberculosis* H37Rv Strain

For the antitubercular evaluation, two growth media were used, viz., (i) 7H9/ADC/Tw comprising of Middlebrook 7H9 broth base with 0.2% glycerol, 0.2% glucose, 0.5% BSA fraction V, 0.08% NaCl, and 0.05% Tween 80; and (ii) 7H9/glucose/casitone/Tx that contained the same broth base with 0.4% glucose, 0.03% Bacto casitone, 0.08% NaCl and 0.05% tyloxapol. Round-bottom 96-well plates were used to perform the assay wherein 50 µL of the chosen media was added to each well, with or without a serial dilution of the compounds, followed by the addition of 50 µL of diluted *M. tuberculosis*. The final concentration achieved was 1 x 10^4 cfu per well and the concentrations of the final compounds ranged from 50-0.024 µM. The bacterial growth was monitored after 1 and 2 weeks using an inverted enlarging mirror plate reader post incubation at 37°C. DMSO was used as the standard solvent, and isoniazid, rifampicin, and ethambutol, were used as the positive controls in the study [28, 38, 39].

2.7 Antitubercular Studies on Clinical Drug-Resistant Strains

The method described in the previous section was followed. The clinical strains used in this study were K33b00MR, 202293, 053K113, 0K113, 0K116, NIH_G4XR, K37b00XR, 28K111, NIH_G367DR, K32b00MR, K29b00MR, NIH_G269DR, and K20b00MR. These MDR and XDR strains are subset of the strains described in Via et al. (2010) [40]. They were resistant to multiple prominent anti-TB drugs (Table 3). These strains were grown in the 7H9/ADC/Tw medium and linezolid was the positive control used. We tested the compounds 5b, 5c, 5e, 5f, 5h, and 5i against these strains [41].

2.8 *iniBAC* promoter induction study

The assay using the reporter strain where the *iniB* promoter drives expression of the *luxCDABE* genes were performed (in7H9/glucose/casitone/Tx medium) as previously described [42]. Briefly, the cells were grown up to OD_{650nm} of 0.2 in 7H9/glucose/casitone/Tx + kanamycin at 25 µg/mL and then diluted to $OD650_{nm}$ of 0.04 in the same medium. An equal volume of cells (50 µL/well) was added to 50µL of the same medium containing the compound as a serial 2-fold dilution series in duplicate. Compounds were tested from 50 µM down to 0.049 µM along with a drug-free control. This was done in sterile flat-bottom white

plates. Luminescence was recorded on days 1, 2, 4 and 7. The positive controls (standards) used in this assay were isoniazid and SQ109.

3. Results and Discussion

3.1 Homology Model Quality and Protein Pocket analysis

The Ramachandran Plot of the optimized homology model showed that there were hindered residues lying in the disallowed regions of the plot. LYS535, LYS504, and GLU378 were the three non-proline and non-glycine residues which lied in the disallowed region (Fig. 2A). Upon performing loop refinement with Prime on the desired residues, a new plot was obtained which clearly showed that the concerned residues were corrected to their relaxed states. There were no residues other than proline and glycine which lied in the disallowed regions thus ensuring the quality of the model (Fig. 2B).

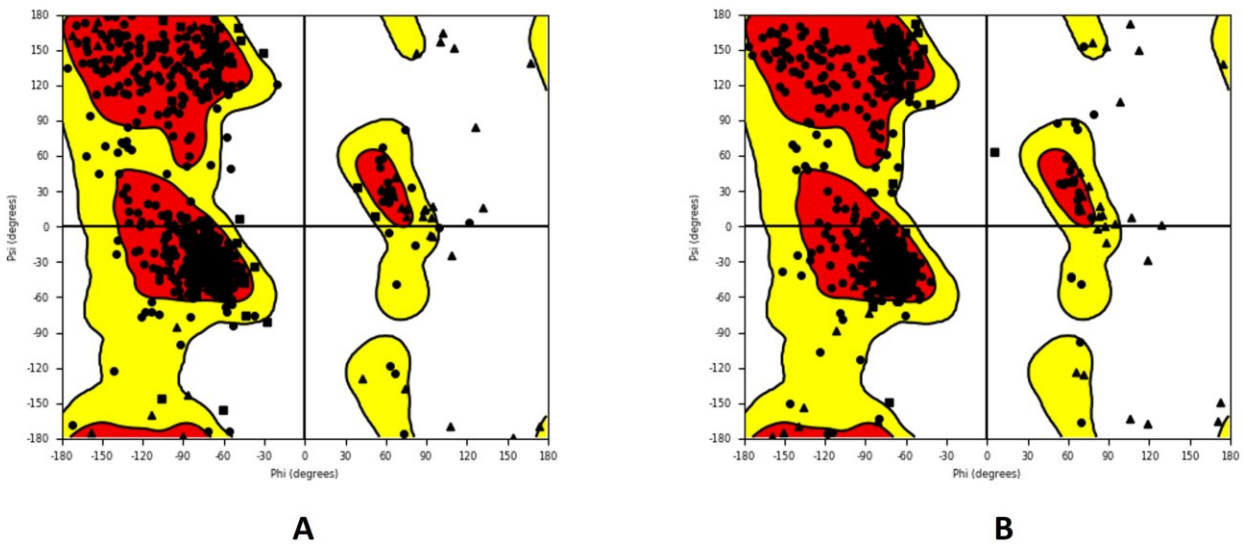

Fig. 2 (A) Ramachandran Plot before loop refinement in MOD2. (B) Ramachandran Plot after loop refinement in MOD2. Red, yellow, and white plot regions indicate unfavoured, allowed and favoured regions, respectively. Glycine residues are represented by dark squares whereas proline residues are represented by dark triangles. Dark round blocks represent non-glycine non-proline residues

The RMSD plot clearly revealed that the system got equilibrated at around 25 ns and was stable thereon (Fig. 3A). The ligand RMSD was within the range of 1 Å throughout and hence it could be asserted that the protein residues at the binding site was devoid of improperly modelled conformations or orientations. In the RMSF plot, spikes were only observed in the loop regions. It is to be noted that the loop regions post residue number 710

were not modelled to avoid large deviations. The binding regions (shown in green lines) comprised majorly of secondary structures of the protein (overlaid on pink and blue). The highest value of RMSF in the protein was ≈ 4.5 Å for residues 345-350 (Fig. 3B). The secondary structure consistency (alpha-helix shown in orange and beta-pleated sheets shown in blue) was fairly high throughout the assessment for all the concerned residues. With all the parameters satisfying the validation criteria, this model was considered highly reliable and the docking and molecular dynamics studies were carried on with it thereafter (Fig. 3C).

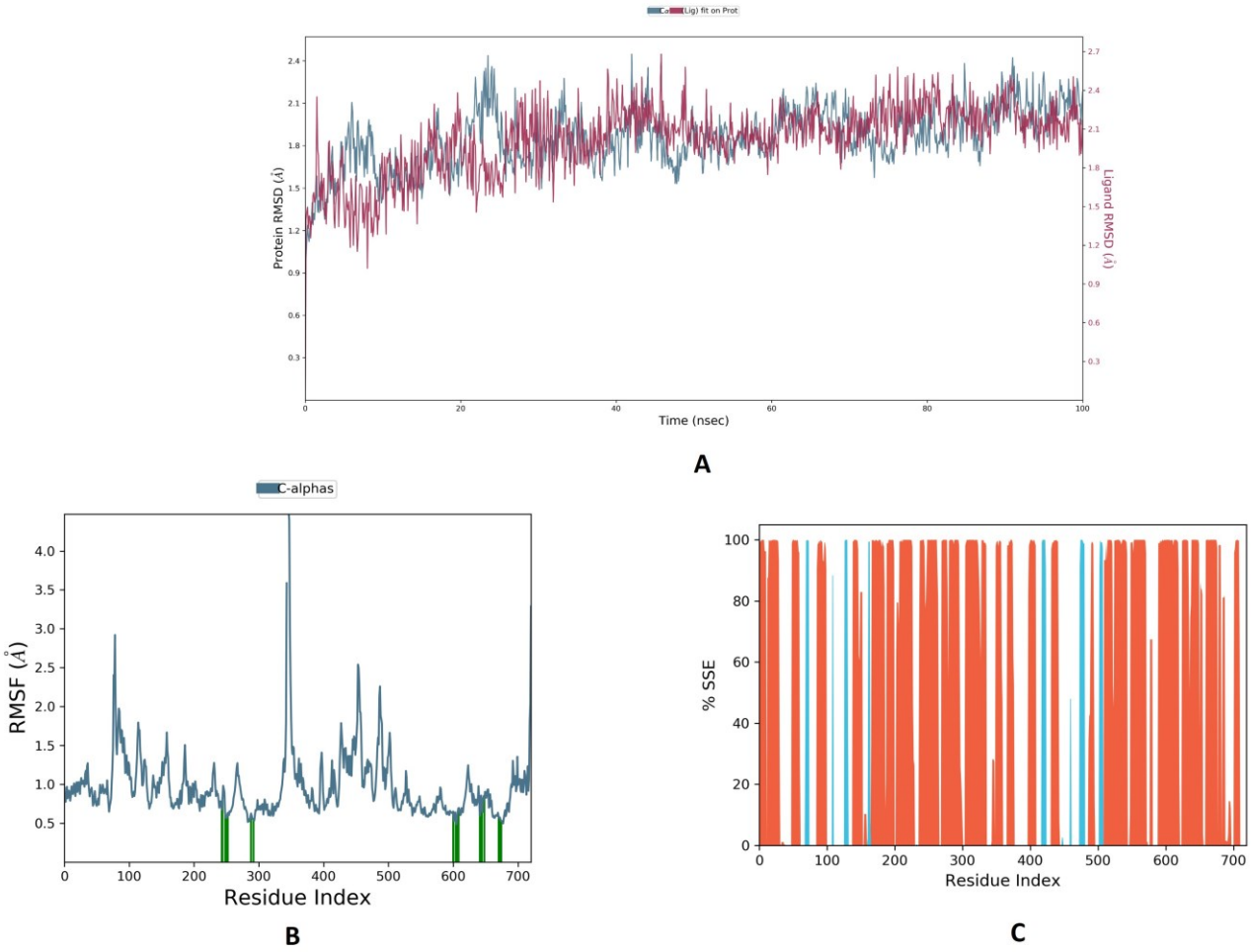

Fig. 3 (A) RMSD plot for MmpL3-rimonabant (MOD2) complex for 100 ns simulation time. (B) RMSF plot for MmpL3-rimonabant (MOD2) complex for 100 ns simulation time. Green lines intersect on residues taking part in active binding with the ligand. (C) Secondary structure evaluation for MmpL3-rimonabant (MOD2) complex for 100 ns of the simulation time. Orange, blue, and white regions represent alpha helix, beta-pleated sheets, and loop regions, respectively

3.2 Docking

Compounds 5b, 5e, and 5h, exist as mixtures of four stereoisomeric forms. The possible isomers of 5h are shown in Fig. 4. Compounds 5c, 5f, and 5i, on the other hand, were mixtures of only two of their geometrical isomers i.e., cis and trans, since the compounds lacked chiral centres. The isomers of 5i are shown in Fig. 5. The isomeric forms of 5b, 5e, 5h, and 5f, can be viewed from their docked poses (Fig. S2, S3, S4, S5).

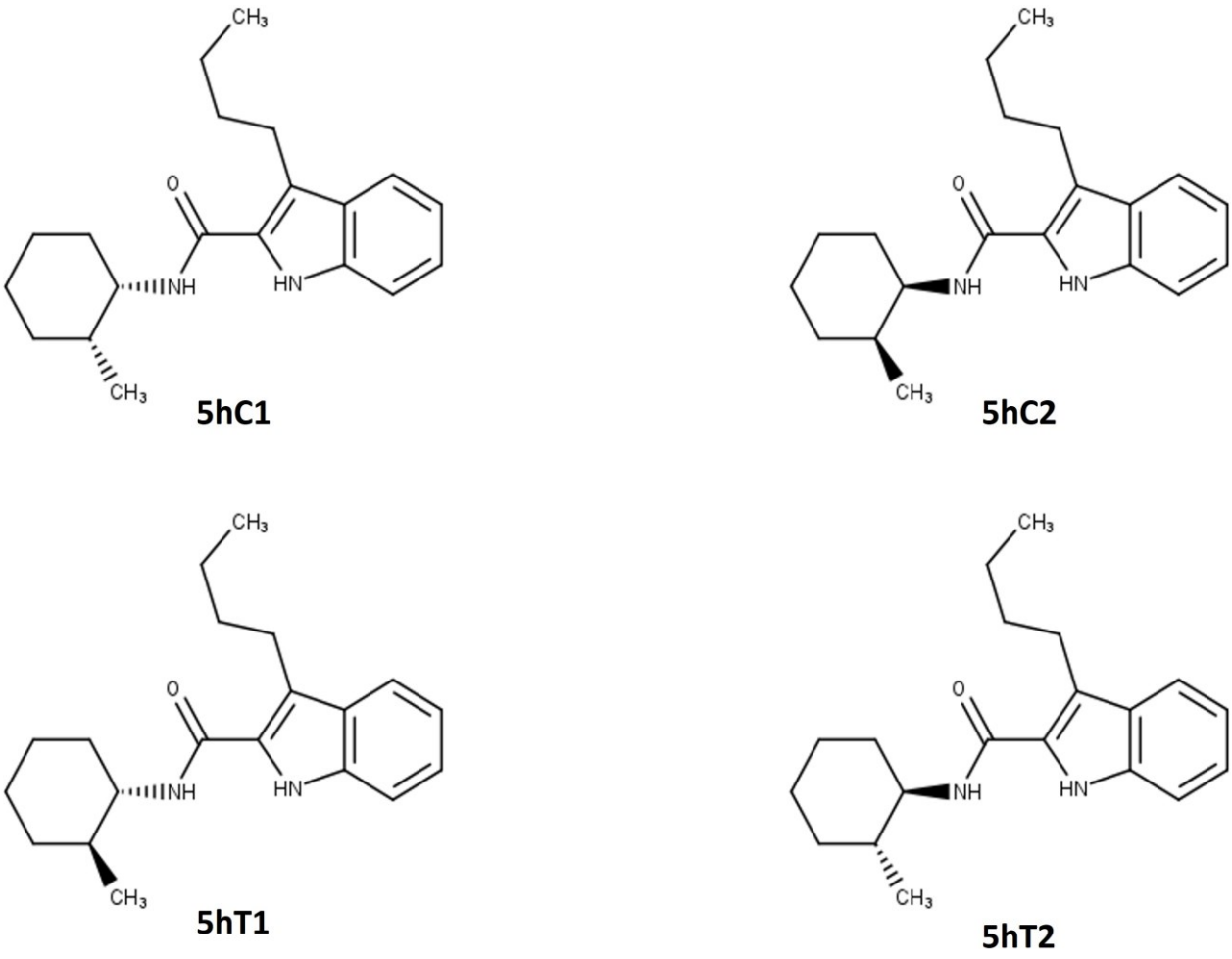

Fig. 4 Stereoismoeric formsof the molecule 5h. C1 and C2 represent the cis-isomers whereas T1and T2 represent the trans-isomers

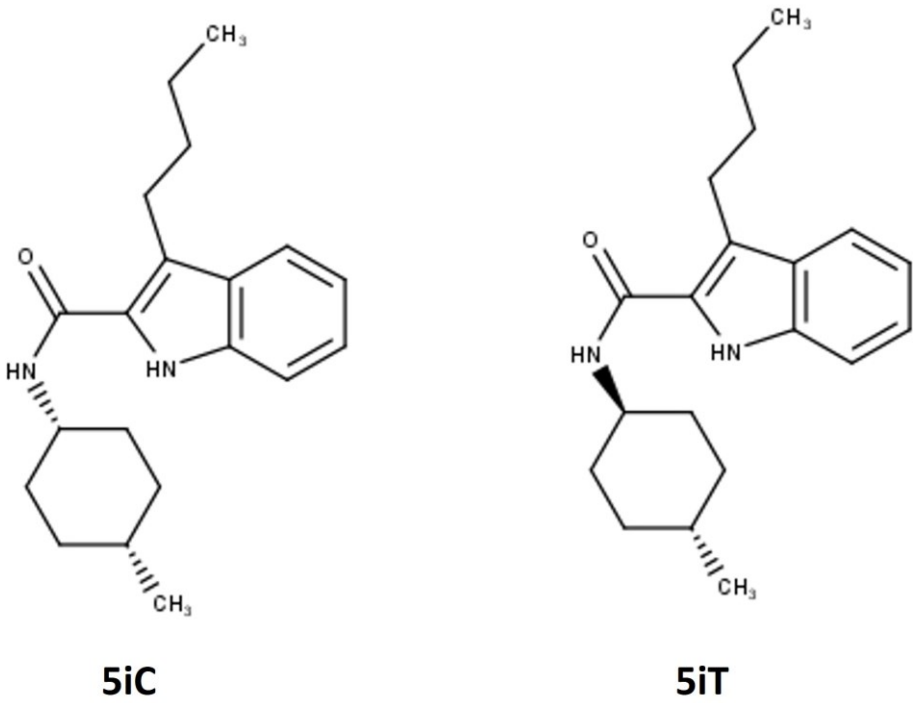

Fig. 5 Stereomeric forms of the molecule 5i. C and T represent cis and trans, respectively

Table 1 illustrates the docking scores and MMGBSA dG bind scores of the molecules that were selected for synthesis. All of them fulfilled our criteria of having a docking score of less than -8 and and a dG bind score of less than -40 kcal/mol. These scores were merely used ensure enrichment and not for any corelation with biological activities. Quite interestingly, the docked poses in the MmpL3 binding pocket did not show any major polar interactions for most of the molecules. The docked poses of 5cT and 5cC are illustrated in Fig. 6. In case of 5cC, the 4-CH_3 cyclohexyl part of the molecule contributed by helping in forming hydrophobic interactions with residues PHE644, TYR641, ILE674, ALA677, and ALA678. The ethyl group at the 3rd position of indole could interact similarly with residues TYR252, LEU707, LEU703, etc. Other important non-polar residues that were in vicinity of the indole ring include ILE248, LEU633, ILE292, and VAL681. Quite intersetingly, no polar interactions were seen with ASH251 and ASP640(Fig. 5B&5C). The interaction pattern were very similar in case of 5cT (Fig. 6C) where the ligand was surrounded by hydrophobic residues and there wasabsence of polar interactions. In case of 5iC and 5iT, the propyl group at third position interacted with residues like VAL681, ALA678, LEU707, MET704, ALA685, ALA682, and LEU703 (Fig. 7A, 7B, & 7C). Non-polar residues like PHE644, TYR641, PHE255, and TYR252 were found to interact with the 4-CH_3cyclohexyl end of the molecule. Similarly, the other end of the molecule, i.e. the indole region, interacted with

hydrophobic residues like LEU637, LEU633, ILE292, and ILE247. Similar to 5c, no polar interaction was seen between the molecules and residues ASP640 or ASH251. Compounds 5a, 5d, and 5g, lacked any methyl group on cyclohexyl and that would imply that they would have poorer binding affinity compared to the other molecules from Scheme 1 (Fig S1). But this couldnot be well established just by analysing the docking or dG bind scores. However, whole cell antitubercular screeing data shows that these molecules had lesser potency compared to those with methyl substituted cyclohexyl moeities (Table 2). Compounds 5b, 5e, and 5h, had methyl substitution on the 2nd position of cyclohexyl ring. Each of these molecules were present as a mixture of two cis and two trans isomers (two diastereomers for each geometrical form). The docking poses of each of the strucutres revealed very similar poses to 5c, 5f, and 5i. There was end to end fitting of these moleculesin the hydrophobic grooves. However, it could be noted that the 2-CH_3 group of cyclohexyl of these moleculescould not form hydrophobic contacts with residues PHE644, TYR641, PHE255, and TYR252 (Fig. S2&S3).The higher MIC vlaues (less active) for 2-CH_3 subsituted (on cyclohexyl) compounds than 4-CH_3 can be justified by same. It has to be noted that although prominent non-covalent hydrophobic contacts could be characterized by the dokced poses, polar interactions, escpecially H-bond interactions, were seldom seen (except for molecule 5bC2 shown in Fig. S2B). The molecule 7c was a good fit in the hydrophobic groove. The third postion of the indole linked with 4-CH_3 benzyl-amino group interacted with a wide array of hydrophobic residues like VAL684, ALA685, PHE688, VAL681, LEU699, ALA700, MET696, and LEU243. The cyclohexyl group was in vicinity of ALA678, ALA677, PHE644, PHE255, TYR252, PHE644, and TYR641, for hydrophobic interactions. On the other hand, ILE244 and ILE248 was in vicinity of the indole ring for simiar non-polar interactions (Fig. 8).

Table 1 Docking score and MMGBSA dG bind scores of the designed and synthesized moelcules.

Sl No	**Comp Code**	**Docking Score**	**MMGBSA (kcal/mol)**
1	5a	-8.03	-41.32
2	5b*	-8.55	-44.13
3	5c*	-8.85	-47.27

4	5d	-8.58	-47
5	5e*	-8.87	-52.21
6	5f*	-8.52	-50.86
7	5g	-9.24	-57.39
8	5h*	-9.31	-57.91
9	5i*	-8.99	-55.73
10	7a	-10.71	-65.63
11	7b	-8.52	-76.39
12	7c	-8.21	-70.89

*Compounds are present as stereo isomeric mixtures. The docking and dG bind scores of thesecompounds are average scores from their isomers.

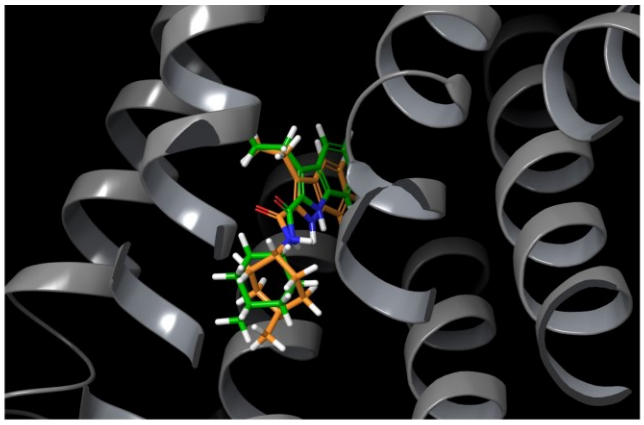

A

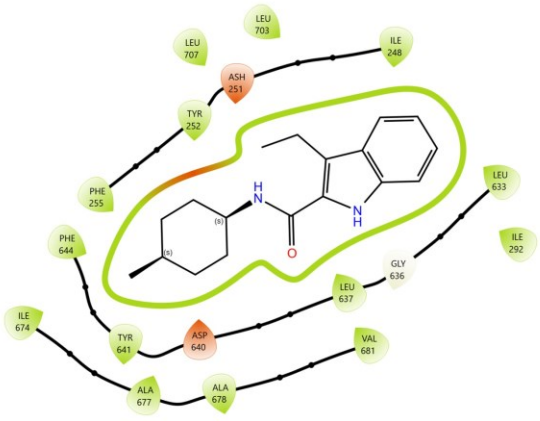

B

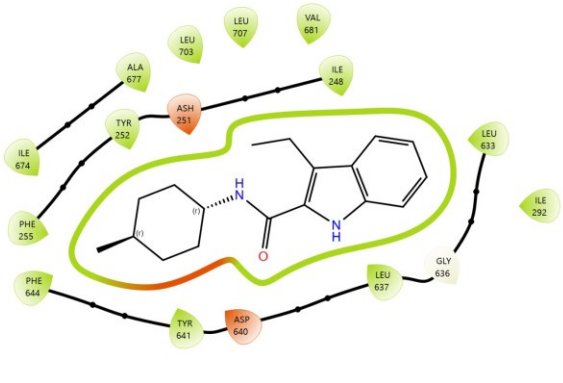

C

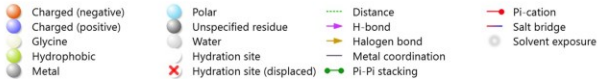

Fig. 6 (A) 3D docked pose of 5cC and 5cT superimposed in MmpL3 binding pocket. The ligands 5cT and 5cC are displayed in colours light brown and green, respectively. (B) 2D docked pose of 5cC in the MmpL3 binding pocket. (C) 2D docked pose of 5cT in the MmpL3 binding pocket.

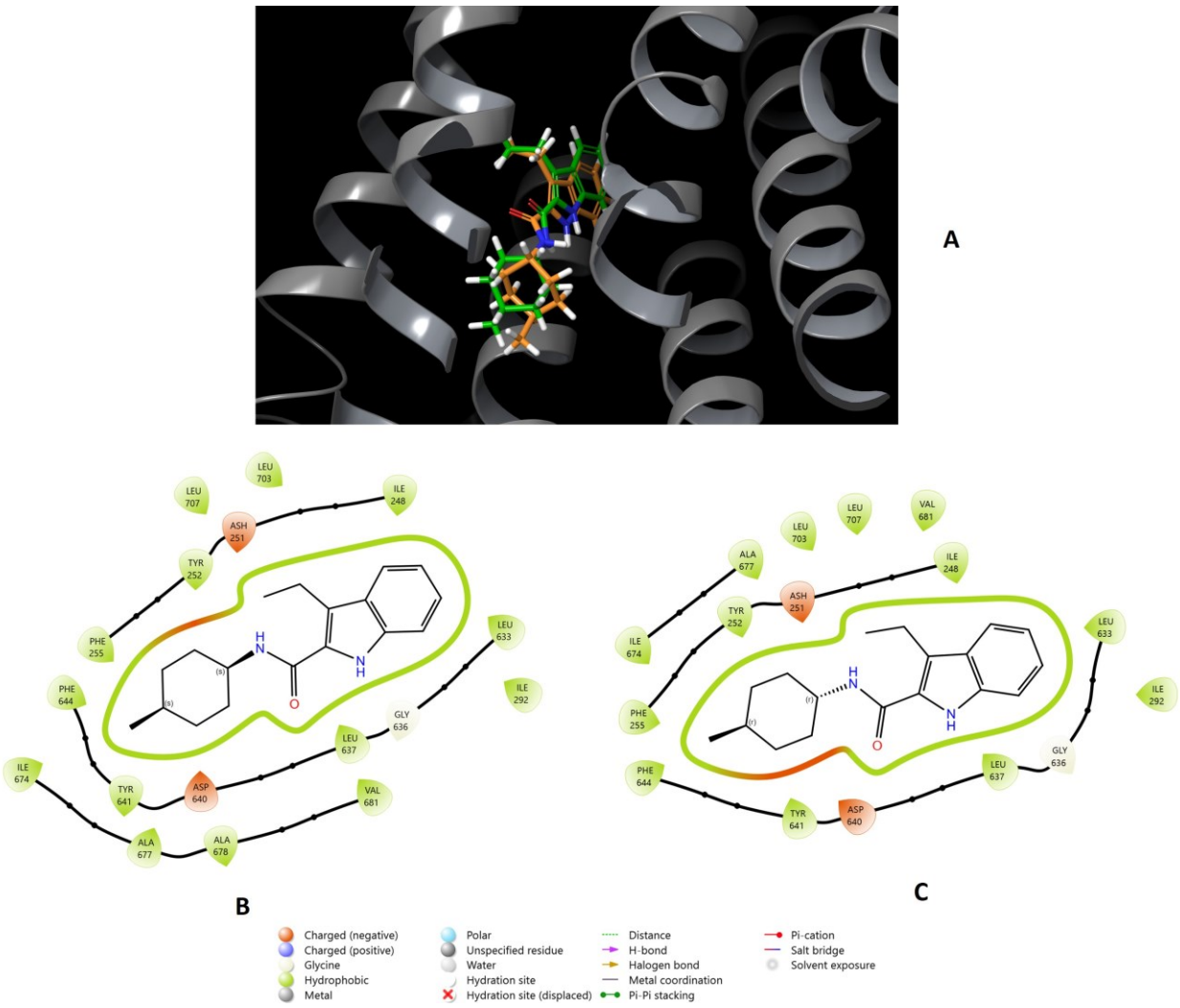

Fig. 7 (A) 3D docked pose of 5iC and 5iT in MmpL3 binding pocket. The ligands 5iT and 5iC are displayed in colours light brown and green, respectively. (B) 2D docked pose of 5iC in the MmpL3 binding pocket. (C) 2D docked pose of 5iT in the MmpL3 binding pocket

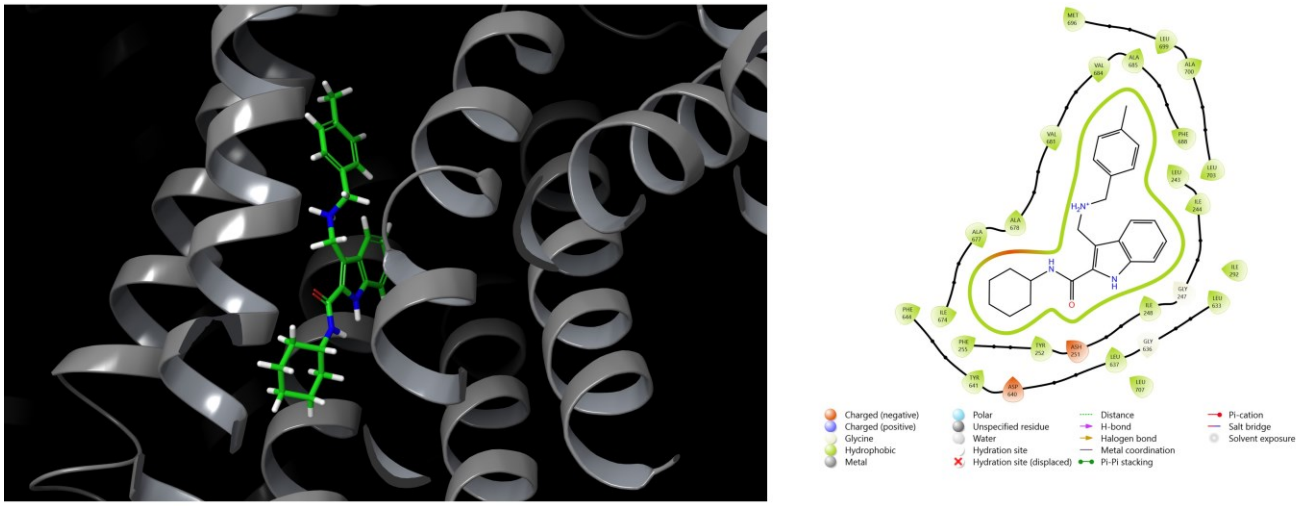

Fig. 8 (A) 3D docked pose of 7c in MmpL3 binding pocket. (B) 2D docked pose of 7c in the MmpL3 binding pocket

3.3 Synthesis and spectral analysis

The synthesis of the compounds 5a-5i (Scheme 1) involved the use of five steps. The first step was an esterification reaction where indole-2-carboxylic acid was converted to its methyl ester. The second step was a classic Fridels-Crafts' acylation reaction resulting in the acylationat the third postion of the indole-2-methyl ester where aluminium chloride was used as the Lewis acid. Therafter, the reduction of the acyl group was performed with the help of triethyl silane followed by the hydrolysis of the ester back to its carboxylic acid form. The esterification was essential for the acylation and the subsequent reduction step. Finally, the alkyl subsituted indole-2-carboxylic acids were converted to their subsequent amides with the help of acid-amine coupling reactions. EDC.HCl and HOBt were conviniently used as the coupling agents to perform the final step. We could confirm the synthesized compounds by analyzing the ^{1}HNMR, ^{13}CNMR, and Mass spectra (see Supplementary Information). One of the characteristic peaks in ^{1}HNMR for the Scheme 1 compounds would be for the cyclohexyl C-H attached to the amide N. It showed up as multiplet in the range of 4.5-3.5 ppm. The indole ring N-H would show up the in the range of 11.3-9 ppm as either a singlet or a combination of two singlets. The characteristic aliphatic peaks were seen in the range of 2.2-0.5 ppm. These mainly comprised of the C-Hs of the cyclohexyl ring and the alkyl chain at the 3rd postion. The peaks for the methylene protons attached to the 3rd positon of the indole ring were shifted and was seen in the range of 3.1-2.8 ppm (Fig. S7-S18). As discussed

earlier, that except for 5a, 5d, and 5g, all the other final compounds from Scheme 1 were present as mixtures of their corresponding isomers. This was clearly evident form their ^{1}HMR and ^{13}CNMR spectra. One such example is 5f, where two singlets were observed at 9 ppm and 8.96 ppm, two doublets at 6.28 ppm and 5.58 ppm, and two multiplets at 4.36 ppm and 3.95 ppm (Fig. S12A-C). This phenomenon of pseudo-splitting would be most likely due to the presence of the cis and trans isomers of 5f (5fC and 5fT) where the characetrsitic peaks of each isomer would appear with slightly different chemical shifts. Similarly, the-CH_3 protons from cyclohexyl ring appear as two doublets instead of a single one due to isomeric forms (Fig. S12B). Similar pseudo-splitting pattern was observed with the peaks for C=O, aromatic Cs, and aliphatic Cs, in the ^{13}CNMR of the compounds. The most distinct separation was observed for the cyclohexyl C attached to amide N at 48.45 ppm and 45.90 ppm (Fig. S12D). These spectral observations in ^{1}HNMR and ^{13}CNMR were consistent for 5c and 5i (Fig. S9&S15). The pseudo-splitting was also observed for compunds 5b, 5e, and 5h, although it was less prominent. In case of 5h, two peaks for the indole N-H were seen at 11.27 ppm and 11.07 ppmin the ^{1}HNMR (Fig. S14A&C). Two multiplets in the range of 4.14-3.58 ppm accounted for the cyclohexyl C-H attached to the amide N (Fig. S14A&B). Also, in the ^{13}CNMR, the same carbon showed two peaks at 53.99 and 49.49 ppm (Fig. S14D).Quite expectedly, the splitting pattern was completely absent in the spectra of 5a, 5d, and 5g. (Fig. S7, S10, & S13). The LC-MS data revealed prominent M-1 peaks for all the final compounds of Scheme 1 (5a-5i) (Fig. S7D, S8D, S9C, S10D, S11C, S12E, S13C, S14E, & S15F). The first step of Scheme 2 (7a-c) involved the synthesis of cyclohexyl indole-2-carboxamides from indole-2-carbolxylic acid. The standard procedure used in Scheme 1 was followed. In the next step, a Mannich type reaction was carried out in acetic acid with the indoleamide, formaldehyde, and the respective amines. Apart from the common characteristic peaks as seen for compounds 5a-5i, few distinctive ^{1}HNMR and ^{1}CNMR peaks were also observed in the Scheme 2 compounds (Fig. S16-S18) . These included a doublet at 4.54 ppm for 7a, that corresponded to methylene protons attached to phenylamine group (Fig. S16A&B). Two singlets, one at 4.06 ppm, and the other at 3.73 ppm were observed for 7b, and a singlet and doublet at 3.98 ppm and 3.66 ppm, respectively, for 7c (Fig. S17A&S18A). These peaks corresponded to the two methylene protons attached to either sides of amine N. The amine attached methylene carbon peaks showed up at 38.16 ppm for 7a (Fig. S16D), 47.48 ppm and 41.44 ppm for 7b (Fig. S17B), and 48.08 ppm and 42.22 ppm for 7c (Fig. S18B). In the LC-MS data of these compounds, the corresponding M+1 peaks were observed along with their coressponding fragmentation peaks (Fig. S16E, S17C, &S18C).

3.4 In vitro Antitubercular Activity against H37Rv

The antitubercular activity of all the synthesized molecules are illustrated in Table 2. For the majority of the synthesized compounds, there was evidence of protein binding being detrimental to activity since the potency was superior in the BSA-free7H9/glucose/casitone/Tx medium. Compounds 5a-5i exhibited MICs of less than 10 µM. Quite significantly, 5c (MIC = 0.39 µM), 5f (MIC = 0.78 µM), and 5i, had MIC values of less than 1 µM. This was expected as all the three molecules had a methyl substitution at the 4th position of cyclohexyl ring of the indole-carboxamide and our previous studies had shown a methyl group at the 4th position was more favourable than this substitution at the 2nd position. However, 5c with an ethyl substitution at the 3rd position of indole, had the best potency (compared to propyl or butyl substituted indole at 3rd position, i.e., 5f and 5i, respectively). We tried to address this with the help of MD studies (vide infra). Among the compounds 7a-c, only 7c showed significant potency (MIC = 4.7 µM), where most likely, the presence of a methyl group at the 4th position of the benzyl part favoured potency. Whereas substitution with 4-Cl on phenyl ring in case of 7a, and 4-Cl on benzyl ring, considerably reduced the activity. Among the positive controls used, isoniazid (INH), rifampicin, and ethambutol exhibited MICs of 0.15 µM, 0.058 µM, and 3 µM, respectively, in 7H9/glucose/casitone/Tx medium.

Table 2 Determined antitubercular activity of the synthesized compounds in different media.

Sl No.	Code	Molecular Weight	1-week MIC in 7H9/ADC/Tween 80 (µM)	1-week MIC in 7H9/glucose/casitone/ Tyloxapol (µM)
1	5a	270.3	12.5	9.4
2	5b	284	12.5	3.13
3	5c	284	3.13	0.39
4	5d	284.3	25	6.25
5	5e	298.4	25	4.7
6	5f	298.4	3.13	0.78

7	5g	298.4	19	9.4
8	5h	312.5	12.5	6.25
9	5i	312.5	4.7	0.6
10	7a	382	>50	>50
11	7b	396	>50	25
12	7c	375.5	>50	4.7
	Isoniazid		0.3	0.15
	Rifampicin (µM)		0.007	0.058
	Ethambutol		1.5	3

3.5 In Vitro Antitubercular screening against resistant strains of *M. tuberculosis*

Three of the most potent compounds that showed activity against H37Rv strain i.e., 5c, 5f, and 5i, were evaluated against various drug-resistant strains. Antitubercular activity of the compounds 5c, 5e, and 5i against various drug-resistant strains are illustrated in Table 3. A total of 13 different MDR, MDR+ and XDR strains were used for testing the antitubercular activity of the compounds. 5c, 5f, and 5i, were found to be potent against these strains suggesting that pre-existing resistance is not a concern for the development of these compounds.

Table 3 Determined antitubercular activity of three selected molecules against drug resistant strains.

Sl No	**Strain name**	**Clinical phenotype**	**DST**	**MIC in µM**			
				5c	**5f**	**5i**	**Linezolid**
1	K33b00 MR	MDR+	HREZSKPTh	3.13	6.25	4.7	0.78
2	202293	MDR+	HRKSP, Eta, EMB	3.13	6.25	6.25	0.78
3	053K113	XDR	HRSKPZO, Cap, Amk, Pth, Mfx, Lev, Rbu, LZD	2.3	4.7	3.13	25

4	0K113	XDR	HRSKPZO, Cap, Amk, Pth, Mfx, Lev, Rbu,	2.3	3.13	3.13	12.5
5	0K116	XDR	HRESO, Pth, Cs, Mfx, Lev, Rbu	6.25	6.25	4.7	0.78
6	NIH_G4 XR	XDR	HREPKOTh	3.13	6.25	4.7	0.6
7	K37b00 XR	XDR	HREKPZO, Mox, Lev, Rbu	3.13	4.7	3.13	0.6
8	28K111	XDR	HRESKPZO, Cap, Amk, Pth, Cs, Mfx, Lev, Rbu, LZD	6.25	6.25	6.25	50
9	NIH_G3 67DR	MDR+	HRXMfx	4.7	9.4	4.7	0.6
10	K32b00 MR	MDR+	HRKZ, Cap, Amk, Pth, Cs	3.13	6.25	3.13	0.78
11	K29b00 MR	MDR	HRSPO	6.25	9.4	6.25	1.2
12	NIH_G2 69DR	MDR	HRERbu	4.7	9.4	6.25	0.78
13	K20b00 MR	MDR+	HREZSKP	6.25	12.5	6.25	1.2

Note: - H – Isoniazid, R – Rifampicin, E – Ethambutol, Z – Pyrazinamide, S – Streptomycin, K – Kanamycin, Pth – Prothionamide, Cap – Capreomycin, Amk – Amikacin, LZD – Linezolid, O – Ofloxacin, Mfx – Moxifloxacin, Cs – Cycloserine, Rbu – Rifabutin, DST – Drug susceptibility testing.

3.6 *iniBAC* operon induction study

Transcriptional upregulation of the *iniBAC* operon occurs during inhibition of cell wall biogenesis including inhibition of MmpL3 [42]. We were able to demonstrate that the

compounds induced the *iniBAC* operon using the reporter strain where the *iniB* promoter drove the expression of the *luxCDABE* operon resulting in auto luminescence during inhibition of cell wall biogenesis (Fig. 9) [43]. Our data support the notion that these inhibitors target MmpL3.

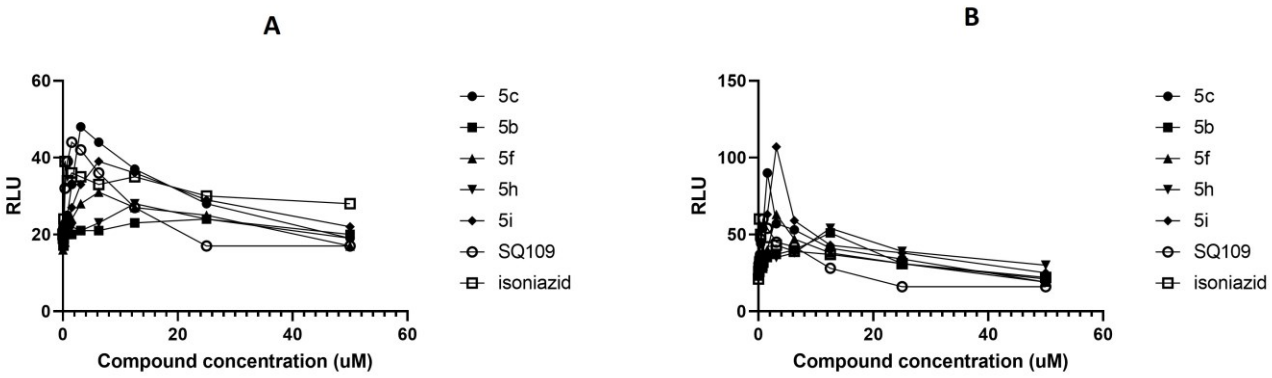

Fig. 9 Cell wall reporter assay showing induction of the *iniBAC* operon during treatment of *M. tuberculosis* with the indole-carboxamides. *M. tuberculosis* expression the *luxCBADE* genes under control of the cell wall inhibition responsive *iniB* promoter was treated with the compounds and luminescence recorded on day 1 (A) and day 2 (B) of treatment. RLU, relative luminescence units

3.7 Molecular Dynamics Simulations: Classical MD vs Simulated annealing

We hypothesized that simulated annealing (SA) simulations would result in the system being in a much lower state than in the case of classical MD simulations. The reason being the fact that this method enables the biomolecular system to cross energy barriers and fall in deeper energy wells which would otherwise be not possible through classical simulations. The highest temperature reached in this method was 410 K. In the following example (trans-isomer of 5f i.e., 5fT), we could demonstrate that the method did not disintegrate the protein when subjected to high temperatures. The protein stability parameters of both the methods produced from the simulations were compared to prove the same. It was observed that the RMSD of the protein in the classical simulation hovered from 2.4 Å to 3.2 Å in the equilibrated state. The RMSD ranged from 2.0 Å to 2.8 Å for the SA-based MD in the equilibrated state (30 ns onwards) (Fig. 10A). Clearly, there was no difference in protein structural stability in the SA method when compared to the classical one (Fig. 10A&11A). Moreover, lesser deviations in SA indicated that the protein might be at a stabler state. Similarly, there was no difference in the secondary structure consistency (SSE plot) between both the methods (Fig. 10B&11B). It was very evident from these observations that high

temperatures attained during the SA simulations did not affect the structural integrity of the protein over the simulation time.

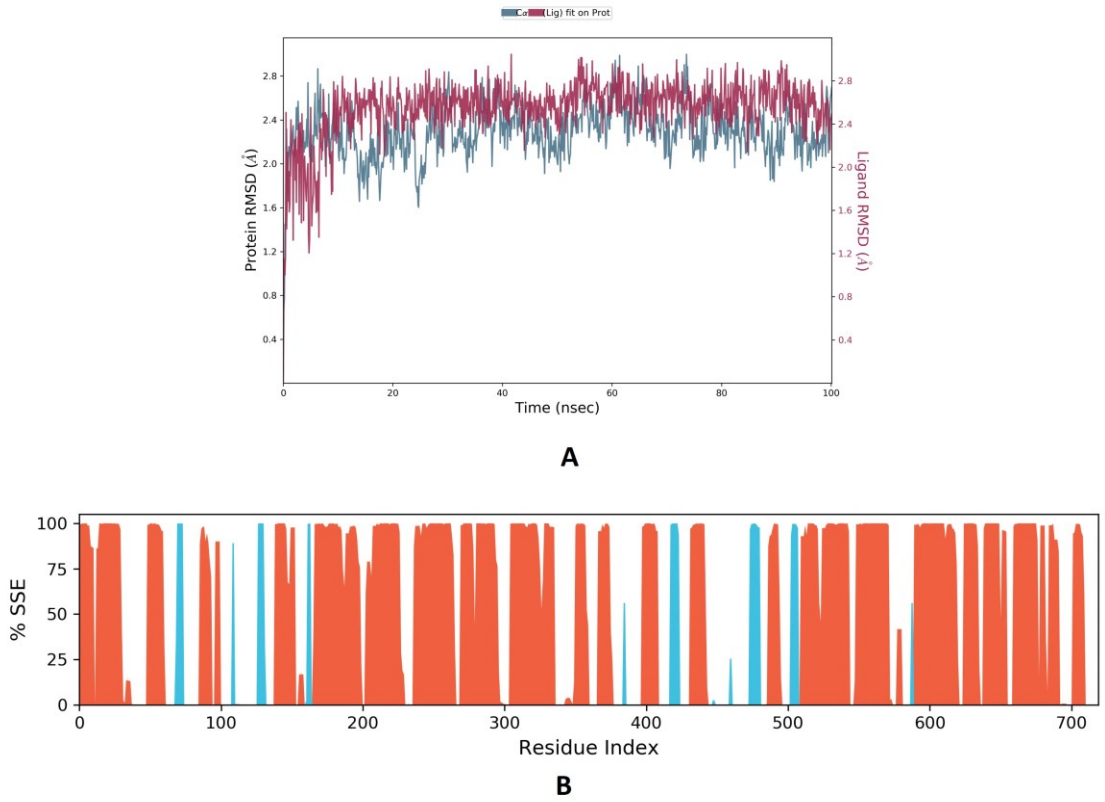

Fig. 10 (A) RMSD plot for 5fT-MmpL3 complex for the simulated annealing-based MD. (B) Secondary structure evaluation for the respective residue indexes for the simulated annealing-based MD. Blue strands represent β-pleated sheets whereas orange strands represent α-helices

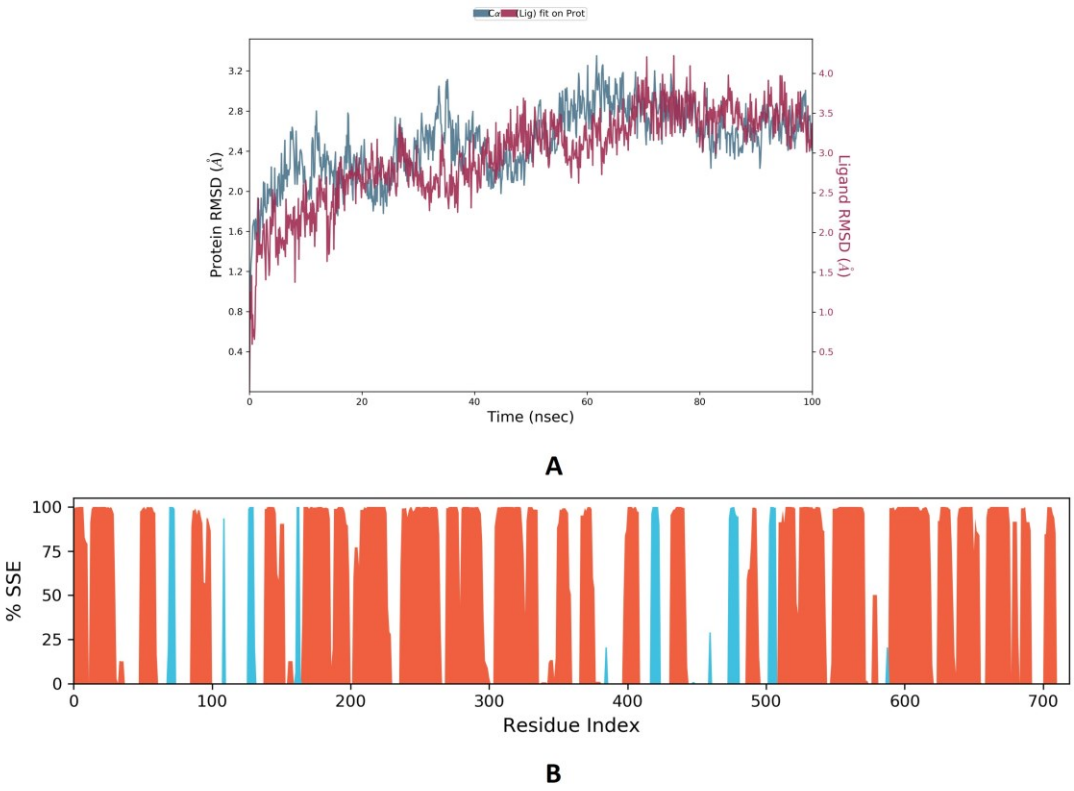

Fig. 11 (A) RMSD plot for 5fT-MmpL3 complex for the classical simulation. (B) Secondary structure evaluation for the respective residue indexes for the classical simulation. Blue colour strands represent β-pleated sheets whereas orange strands represent α-helices

The potential energies were compared for both the methods. The average potential energy for the classical method was found to be 676687 kcal/mol and 676107 kcal/mol for SA. A difference of 580 kcal/mol clearly suggested that the complex through SA was able to attain much lower energy levels than classical. On top of that, the deviations in potential energy were much lower in case of SA (Fig. 12). This indicated that a stabler complex was achieved from SA. Based on these findings, it was clear that the SA method would give superior results from simulations and thus it was selected for carrying out the MD simulations for the remaining complexes.

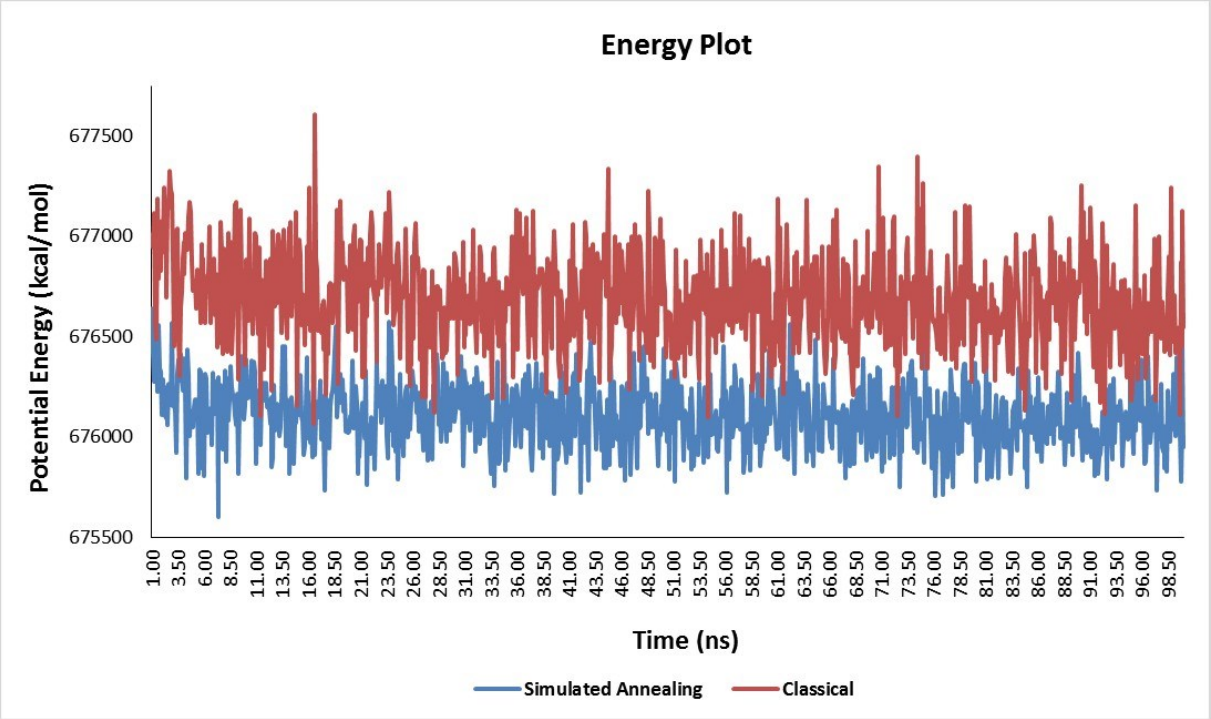

Fig. 12 Potential Energy vs Time (ns) plot of 8fT-MmpL3 complex for the simulated annealing and classical MD method

3.8 Simulated annealing and post-MD MMGBSA

SA-based MD simulations were performed for 5c-MmpL3 and 5i-MmpL3 complexes to gain a better knowledge about the protein ligand interactions. The docked poses were taken as the starting structures for simulation. Each isomer was considered, so essentially, it resulted in four complexes for 5c and 5i. i.e., 5cT-MmpL3, 5cC-MmpL3, 5iT-MmpL3, and 5iC-MmpL3. The dG bind scores of 5c and 5i from the simulated complexes were -67 kcal/mol and -73.2 kcal/mol, respectively. The dG bind scores of the same molecules were -47.27 kcal/mol and -55.73 kcal/mol, respectively from their docked poses (Table 4). The difference could be explained by the fact that well equilibrated SA simulations accounted for the multiple H-bond interactions that the docking studies were unable to generate (Fig. 6-9, 13-16). Thus, the results from the SA studies were considered more reliable and the interactions observed were analysed further.

All the properties related to the interactions of the simulated complexes were calculated post their time of convergence (Fig. S19). The SA results of 5cT show prominent H-bond interactions between ASP251 and amide C=O (97%), ASP640 and indole ring N-H (84%), and ASP640 and amide N-H (77%) (Fig. 13A). In case of 5cC, these very interactions were also present for 98%, 100%, and 97% of the time (Fig. 13A). For 5cT, significant

hydrophobic contacts were contributed by residues TYR641 and ILE292 (Fig. 14A). The interaction histogram reveals that ILE292 and TYR641 showed those interactions for at least 50% and 25%, respectively, of the total simulation time (Fig. 13B). In case of 5cC, it was TYR641, PHE644, and ALA677, that participated through hydrophobic contacts (Fig. 14A). Interactions with ILE292 were present for at least 50% of the simulation time while TYR641 and PHE644 showed interactions for around 30% of the simulation time (Fig. 14B). For 5iC-MmpL3 and 5iT-MmpL3, the simulation converged at 20 ns and 60 ns, respectively (Fig. S16D&C). The remaining properties were analysed post their times of convergence. In case of 5iT, it could be seen that ASP640 formed two essential H-bonds with indole ring N-H and amide N-H for 100% and 89% of the time, respectively. Similarly, ASP251 formed a H-bond with amide C=O for about 95% of the time. Significant hydrophobic interactions existed between the residues ILE292 and LEU637 and the indole aromatic region, and, PHE644 and ALA677 and the substituted cyclohexyl ring (Fig. 15A). The residues involved in hydrophobic contacts, like ILE292, LEU637, PHE644, and ALA677, interacted for at least 25%of the simulation time (Fig. 16B). For 5iC, ASP640 (100% and 89% of the time with indole N-H and amide N-H, respectively) and ASP251 (95% of the time with C=O) played similar roles in forming the H-bonds. TYR641, ILE292, and PHE644 were the significant residues showing hydrophobic interactions (Fig. 16A). TYR641 and PHE644 were the two residues which showed hydrophobic contacts for a minimum of 25% of the simulation time. ILE292, on the other hand showed an interaction of more than 50% (Fig. 16B). These results confirmed the fact that the long ends of these indole-2-carboxamide inhibitors would be rooted in the hydrophobic grooves of MmpL3 (res PHE644, LEU637, ILE292, ALA677, TYR641) supported strongly by anchoring H-bonds with ASP251 and ASP640.

Table 4 MMGBSA dG bind scores from docking and MD.

Sl No.	**Code**	**dG bind in kcal/mol (MMGBSA from docking)**	**dG bind in kcal/mol (MMGBSA from MD frames)**	**MIC (µg/ml)**
1.	5c	-47.27	-67	0.39
2.	5i	-55.73	-73.2	0.60

Note: - Since both 5c and 5i were present as mixtures of their respective geometric isomers, i.e., cis and trans forms, the dG bind scores of each compound are reported as average of their respective isomers' dG bind scores.

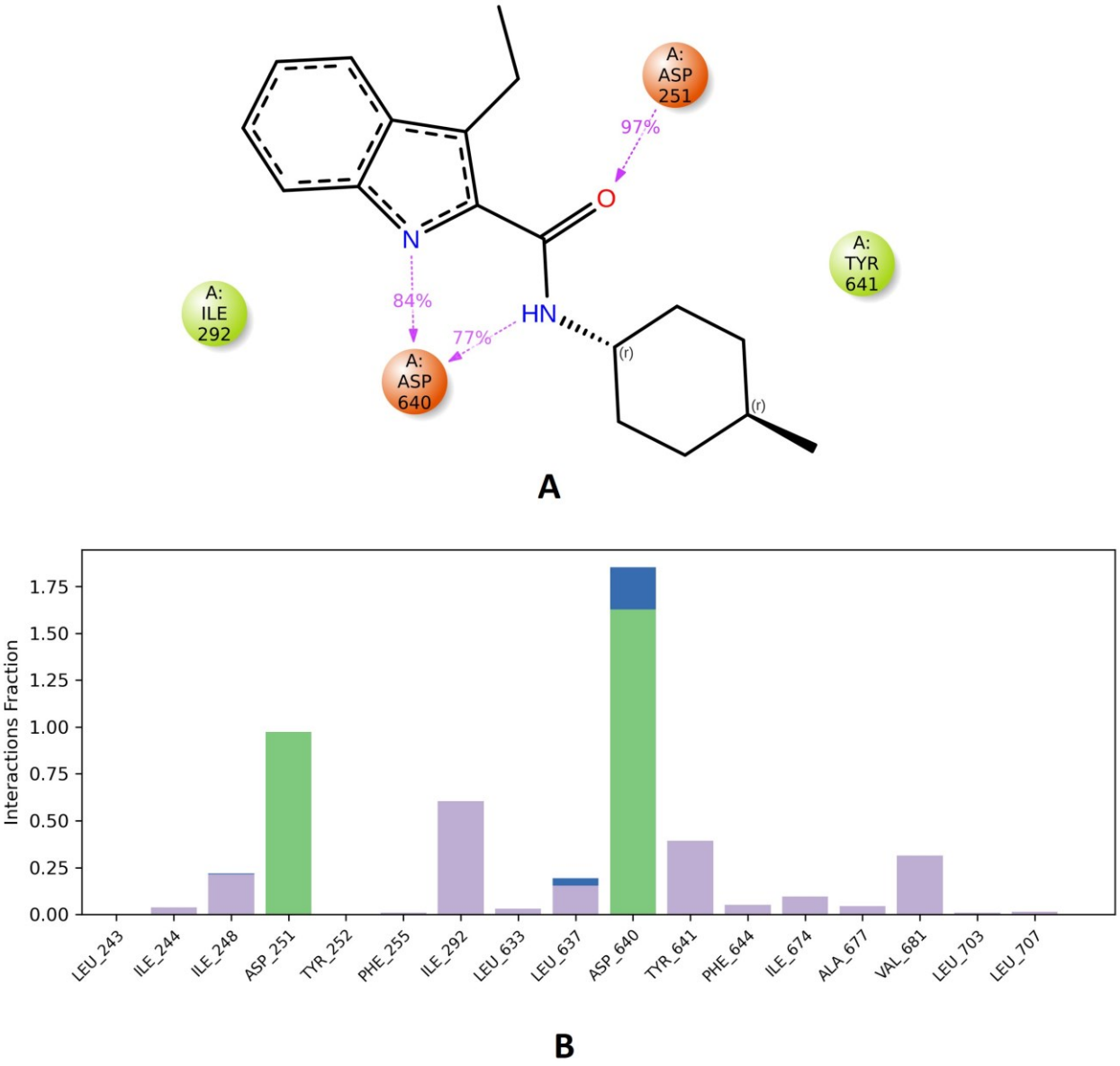

Fig. 13 (A) Protein-ligand contact summary of 5cT-MmpL3 complex. (B) Protein-ligand contact histogram of 5cT-MmpL3 complex

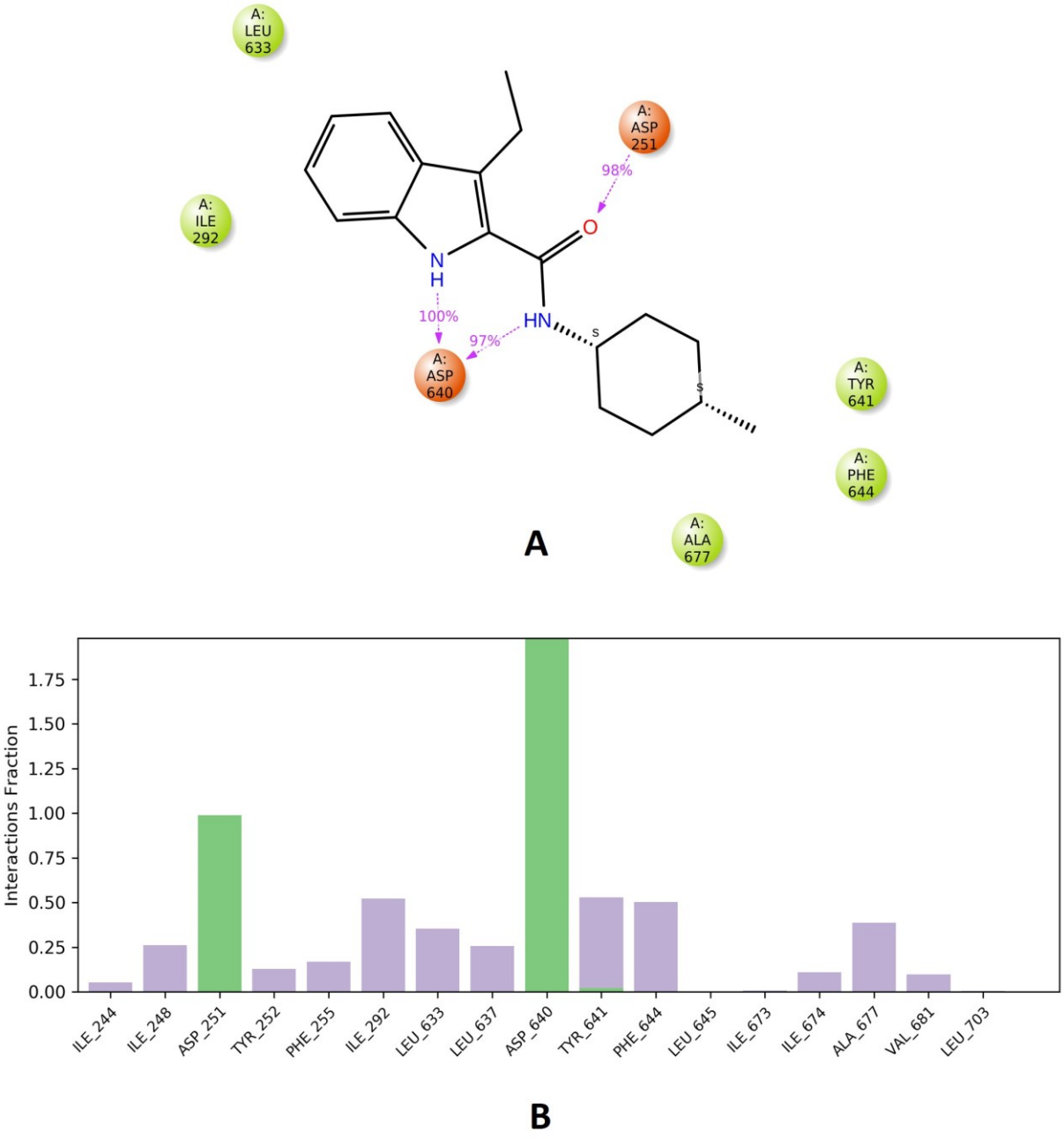

Fig. 14 (A) Protein-ligand contact summary of 5cC-MmpL3 complex. (B) Protein-ligand contact histogram of 5cC-MmpL3 complex

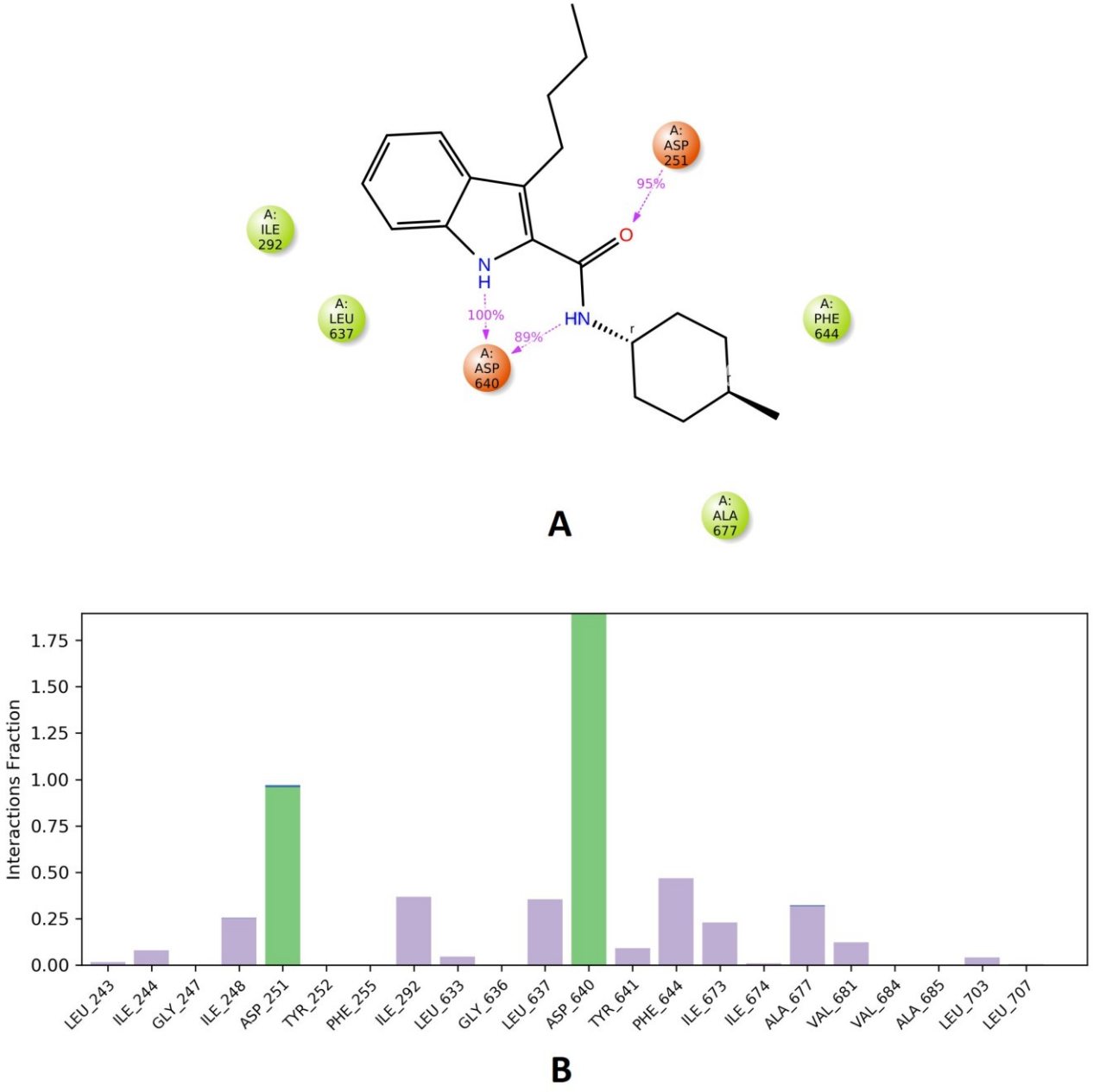

Fig. 15 (A) Protein-ligand contact summary of 5iT-MmpL3 complex. (B) Protein-ligand contact histogram of 5iC-MmpL3 complex

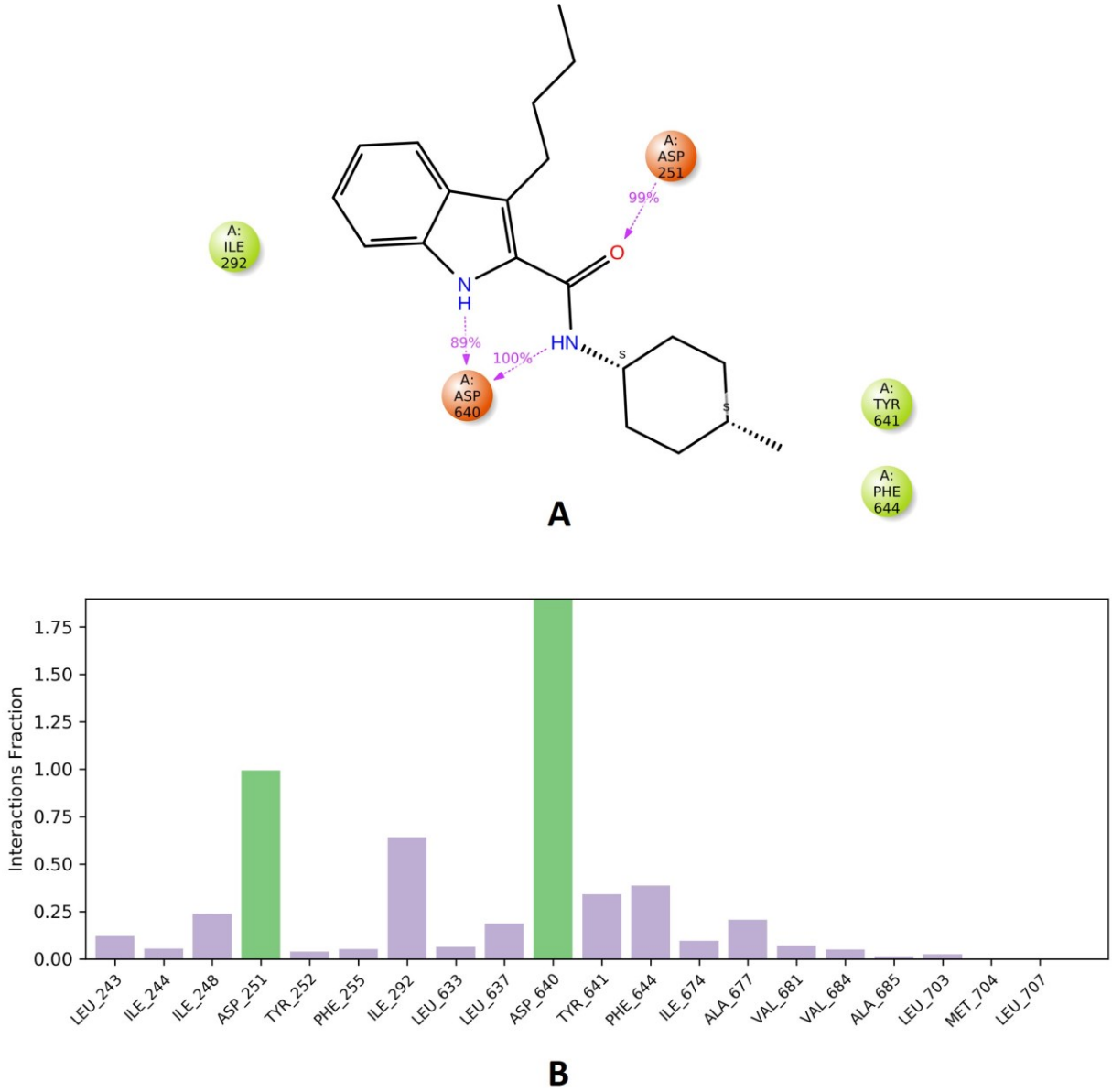

Fig. 16 (A) Protein-ligand contact summary of 5iC-MmpL3 complex. (B) Protein-ligand contact histogram of 5iC-MmpL3 complex

3.9 Insights on protein-ligand binding

From the MIC values against H37Rv strain, and our *iniB-luxCBADE* reporter assay results, as well as extensive molecular modelling studies, it was evident that the potent molecules were likely inhibitors of MmpL3. Additionally, potency of 5c, 5f, and 5i against different drug-resistant strains also indicated that their mechanism of action is different from the currently marketed antitubercular drugs. It was evident from 5a-i series of compounds that alkyl substitution at the 3rd position of indole carboxamides was essential for higher potency of the molecules. Additionally, a methyl substitution at 4th position of cyclohexyl ring favoured the

activity. The dG bind scores from both docking and MD suggested that 8i would have a better binding affinity than 8c. In case of 7a-c series of compounds, 7a and 7b were inactive but 7c was active even though the docking scores and dG bind scores of all these compounds were promising (Table1). Moreover, 7c with 4-CH_3 substitution on the benzyl ring had 5-times more potency than 7b with 4-Cl substitution, although both having an electron rich group at the same position. One possible reason could be the inability of the 4-Cl substituted compounds to penetrate the cell and reach the target. The outcome of whole cell inhibition data depends on multiple factors including access to the target, compound efflux, compound metabolism as well as target engagement.

From the molecular modelling studies, it was observed that at least two H-bond interactions with ASP640 and one with ASP251 are required for the ligands to be have good binding affinity. This meant that the inhibitor ligands had to have at least two H-bond donors and one acceptor at the central part of the molecule. Those interactions were missing in the most of the docked poses of the inhibitor bound complexes. Only the well equilibrated MD simulations could result in the non-covalent polar bond formations. However, the hydrophobic grooves in the pocket and their contacts with the ligands' non-polar regions were also seen in the docked poses. The important residues for hydrophobic interactions from the MD simulations were found to be ILE292, LEU637, and LEU633 in one groove and TYR641, PHE644, ILE244, and PHE255, in the other. This structure supported the end-to-end fitting of the indole-2-carboxamides with indole ring and cyclohexyl ring at each of the grooves. Additionally, bulkier group at the third position of indole was preferred due to the presence of hydrophobic residues like LEU703 and LEU243 ready to form non-polar interactions. Thus, for initial screening of molecules with docking, these hydrophobic residues and interaction of the ligand with them can be set as cut-off parameters when the H-bond interactions are not observed.

4. Conclusion

In this research work, novel indoles were designed, synthesized, evaluated for antitubercular activity. A protein model for Mmpl3 using two templates was developed and validated successfully. Which was used for screening the designed molecules. The docking studies of designed indoles exhibited some necessary interactions. Several of the synthesized compounds showed promising antitubercular potency but most importantly, 3 molecules, i.e., 5c, 5f, and 5i, exhibited excellent antitubercular activity against H37Rv (MIC<1μM) as well

as against different MDR and XDR strains of *M. tuberculosis*. Use of a cell wall reporter assay based on *iniBAC* induction suggested that these molecules were the likely inhibitors of MmpL3. Finally, simulated annealing based MD was performed with selected molecules to gain better insights into the protein-ligand binding modality. This led to the identification of essential residues responsible for polar and non-polar interactions, and the limiting factors for having good binding affinity. Overall, this research has shown promising results but further studies are warranted to ascertain the potency and drug-likeness in later stages of investigation. As a part of future work, the active molecules from the current set can also be further evaluated in vivo to assess their safety and efficacy. Additionally, direct inhibition assay methods for MmpL3 can be utilised in future to absolutely confirm the mechanism of action of the potent molecules.

Article Highlights

- Novel indole-2-carboxamides targeting MmpL3 were designed based on structure-activity relationship (SAR) of previously reported molecules.
- Twelve molecules were synthesized and screened against H3RV strain of *M. tuberculosis*.
- The most potent molecules, 5c, 5f, and 5i, were again tested against multiple MDR and XDR strains of *M. tuberculosis*.
- 5c, 5f, and 5i, were found to be active against the different MDR and XDR strains of *M. tuberculosis*.
- Compounds 5a, 5b, 5c, 5f, and 5i, were also found to induce *iniBAC* operon signifying their probable mechanism through MmpL3 inhibition.
- The docking scores and MMGBSA of all the synthesized compounds were less than -8 and -40 kcal/mol, respectively, signifying good binding affinity for Mmpl3.
- Combining the docking and the simulated annealing studies, it was found that ILE292, LEU637, LEU633, TYR641, PHE644, ILE244, and PHE255 were the important residues for the hydrophobic interactions.
- In addition to the hydrophobic contacts, polar non-covalent interactions with ASP640 and ASP251 were also important for the compounds to show potency.

- From this study, we could consider 5c, 5f, and 5i, as promising antitubercular candidates which supposedly act via inhibiting Mmpl3.

Acknowledgements

The authors would like to acknowledge the facilities provided at Manipal College of Pharmaceutical Sciences, MAHE, India, and the NIAID, NIH, USA, to carry out the research.

Financial disclosure

This work has been funded in parts by AICTE ((RPS File No: 8-77/FDC/RPS) (POLICY-I)|2O19-2O), India, and the Division of Intramural Research, NIAID, NIH, USA.

Competing interests' disclosure

The authors have no competing interests or relevant affiliations with any organization or entity with the subject matter or materials discussed in the manuscript. This includes employment, consultancies, honoraria, stock ownership or options, expert testimony, grants or patents received or pending, or royalties.

Writing disclosure

No writing assistance was utilised for the preparation of the manuscript.

References

1. World Health Organisation (2023). *Global Tuberculosis Report 2023*. [online] www.who.int. Available at: https://www.who.int/teams/global-tuberculosis-programme/tb-reports/global-tuberculosis-report-2023.

2. www.who.int. (n.d.). *WHO Consolidated Guidelines on Tuberculosis, Module 4: Treatment - Drug-Susceptible Tuberculosis Treatment*. [online] Available at: https://www.who.int/publications/i/item/9789240048126.

3. Tballiance.org. (2019). FDA Approves New Treatment for Highly Drug-Resistant Forms of Tuberculosis | TB Alliance. [online] Available at: https://www.tballiance.org/news/fda-approves-new-treatment-highly-drug-resistant-forms-tuberculosis.

4. R Mahajan R. Bedaquiline: First FDA-approved tuberculosis drug in 40 years. Int J Appl Basic Med Res. 2013;3(1):1-2. doi: 10.4103/2229-516X.112228

5. Melly G, Purdy GE. MmpL Proteins in Physiology and Pathogenesis of M. tuberculosis. Microorganisms. 2019;7(3):70. doi: 10.3390/microorganisms7030070

6. Zhang B, Li J, Yang X, Wu L, et al. Crystal Structures of Membrane Transporter MmpL3, an Anti-TB Drug Target. Cell. 2019;176(3):636-648.e13. doi: 10.1016/j.cell.2019.01.003

7. Ma S, Huang Y, Xie F, et al. Transport mechanism of Mycobacterium tuberculosis MmpL/S family proteins and implications in pharmaceutical targeting. Biol Chem. 2020;401(3):331-348. doi: 10.1515/hsz-2019-0326

8. Domenech P, Reed MB, Barry CE 3rd. Contribution of the Mycobacterium tuberculosis MmpL protein family to virulence and drug resistance. Infect Immun. 2005;73(6):3492-501. doi: 10.1128/IAI.73.6.3492-3501.2005

9. Rodrigues L, Cravo P, Viveiros M. Efflux pump inhibitors as a promising adjunct therapy against drug resistant tuberculosis: a new strategy to revisit mycobacterial targets and repurpose old drugs. Expert Rev Anti Infect Ther. 2020;18(8):741-757. doi: 10.1080/14787210.2020.1760845

10. Varela C, Rittmann D, Singh A, et al. MmpL genes are associated with mycolic acid metabolism in mycobacteria and corynebacteria. Chem Biol. 2012;19(4):498-506. doi: 10.1016/j.chembiol.2012.03.006

11. Grover S, Engelhart CA, Pérez-Herrán E, et al. Two-Way Regulation of MmpL3 Expression Identifies and Validates Inhibitors of MmpL3 Function in Mycobacterium tuberculosis. ACS Infect Dis. 2021;7(1):141-152. doi: 10.1021/acsinfecdis.0c00675

12. Xu Z, Meshcheryakov VA, Poce G, et al. MmpL3 is the flippase for mycolic acids in mycobacteria. Proc Natl Acad Sci U S A. 2017;114(30):7993-7998. doi: 10.1073/pnas.1700062114

13. Warrier T, Tropis M, Werngren J, et al. Antigen 85C inhibition restricts Mycobacterium tuberculosis growth through disruption of cord factor biosynthesis. Antimicrob Agents Chemother. 2012;56(4):1735-43. doi: 10.1128/AAC.05742-11

14. Li W, Upadhyay A, Fontes FL, North EJ, et al. Novel insights into the mechanism of inhibition of MmpL3, a target of multiple pharmacophores in Mycobacterium tuberculosis. Antimicrob Agents Chemother. 2014;58(11):6413-23. doi: 10.1128/AAC.03229-14

15. Bailo R, Bhatt A, Aínsa JA. Lipid transport in Mycobacterium tuberculosis and its implications in virulence and drug development. Biochem Pharmacol. 2015;96(3):159-67. doi: 10.1016/j.bcp.2015.05.001

16. Degiacomi G, Benjak A, Madacki J, et al. Essentiality of mmpL3 and impact of its silencing on Mycobacterium tuberculosis gene expression. Sci Rep. 2017;7:43495. doi: 10.1038/srep43495

17. Li W, Obregón-Henao A, Wallach JB, et al. Therapeutic Potential of the Mycobacterium tuberculosis Mycolic Acid Transporter, MmpL3. Antimicrob Agents Chemother. 2016;60(9):5198-207. doi: 10.1128/AAC.00826-16

18. McNeil MB, Cook GM. Utilization of CRISPR Interference to Validate MmpL3 as a Drug Target in Mycobacterium tuberculosis. Antimicrob Agents Chemother. 2019;63(8):e00629-19

19. Bolla JR. Targeting MmpL3 for anti-tuberculosis drug development. Biochem Soc Trans. 2020;48(4):1463-1472. doi: 10.1042/BST20190950

20. Onajole OK, Pieroni M, Tipparaju SK, et al. Preliminary structure-activity relationships and biological evaluation of novel antitubercular indolecarboxamide derivatives against drug-susceptible and drug-resistant Mycobacterium tuberculosis strains. J Med Chem. 2013;56(10):4093-103. doi: 10.1021/jm4003878

21. Kondreddi RR, Jiricek J, Rao SP, Lakshminarayana SB, et al. Design, synthesis, and biological evaluation of indole-2-carboxamides: a promising class of antituberculosis agents. J Med Chem. 2013;56(21):8849-59. doi: 10.1021/jm4012774

22. Zhao H, Gao Y, Li W, Sheng L, et al. Design, Synthesis, and Biological Evaluation of Pyrrole-2-carboxamide Derivatives as Mycobacterial Membrane Protein Large 3 Inhibitors for Treating Drug-Resistant Tuberculosis. J Med Chem. 2022;65(15):10534-10553. doi: 10.1021/acs.jmedchem.2c00718

23. J. Jiricek, R. R. Kondreddy, and P. W. Smith Indole Carboxamide Derivatives And Uses Thereof. World Intellectual Property Organization, International Publication Number WOR 2014/037900 AI. International Publication Number WOR 2014/037900 AI.

24. Lun S, Guo H, Onajole OK, et al. Indoleamides are active against drug-resistant Mycobacterium tuberculosis. Nat Commun. 2013;4:2907. doi: 10.1038/ncomms3907

25. Bhattarai P, Hegde P, Li W, et al. Structural Determinants of Indole-2-carboxamides: Identification of Lead Acetamides with Pan Antimycobacterial Activity. J Med Chem. 2023;66(1):170-187. doi: 10.1021/acs.jmedchem.2c00352

26. Ray R, Birangal SR, Fathima F, et al. Molecular insights into MmpL3 leads to the development of novel indole-2-carboxamide. Mol Syst Des Eng. 2022;7(6):592–606. doi: 10.1039/d1me00122a

27. Ray R, Das S, Lobo M, Birangal SR, et al. A holistic molecular modelling approach to design novel indole-2-carboxamide derivatives as potential inhibitors of MmpL3. SAR QSAR Environ Res. 2022;33(7):551-581. doi: 10.1080/1062936X.2022.2096691

28. Adams O, Deme JC, Parker JL, et al. Cryo-EM structure and resistance landscape of M. tuberculosis MmpL3: An emergent therapeutic target. Structure. 2021 Oct 7;29(10):1182-1191.e4. doi: 10.1016/j.str.2021.06.013

29. Hao GF, Xu WF, Yang SG, Yang GF. Multiple Simulated Annealing-Molecular Dynamics (MSA-MD) for Conformational Space Search of Peptide and Miniprotein. Sci Rep. 2015;5:15568. doi: 10.1038/srep15568

30. Wang MP, Chiu CC, Lu TJ, et al. Indolylbenzimidazole-based ligands catalyze the coupling of arylboronic acids with aryl halides. Appl Organomet Chem. 2018;32(6): e4348. doi: 10.1002/aoc.4348

31. Murakami Y, Tani M, Suzuki M, et al. Synthetic Studies on Indoles and Related Compounds. XII. A Simple General Method for the C-3 Acylation of Ethyl Indole-2-carboxylates. Chem Pharm Bull. 1985;33(11):4707-4716. doi: 10.1248/cpb.33.4707

32. Du XW, Ghosh A, Stanley LM. Enantioselective synthesis of polycyclic nitrogen heterocycles by Rh-catalyzed alkene hydroacylation: constructing six-membered rings in the absence of chelation assistance. Org Lett. 2014;16(15):4036-4039. doi: 10.1021/ol501869s

33. Piscitelli F, Ligresti A, La Regina G, et al. Indole-2-carboxamides as allosteric modulators of the cannabinoid CB_1 receptor. J Med Chem. 2012;55(11):5627-31. doi: 10.1021/jm201485c

34. Stec J, Onajole OK, Lun S, et al. Indole-2-carboxamide-based MmpL3 Inhibitors Show Exceptional Antitubercular Activity in an Animal Model of Tuberculosis Infection. J Med Chem. 2016;59(13):6232-47. doi: 10.1021/acs.jmedchem.6b00415

35. Ma F, Ma L, Lei M, et al. Synthesis of 1,2-disubstituted 1,2-dihydropyrrolo[3,4-b]indol-3(4H)-one derivatives. Monatsh Chemie. 2014;145:1035–1041. doi: 10.1007/s00706-014-1171-3

36. Das B, Kumar JN, Kumar AS, et al. A distinct novel approach for the synthesis of 3-indolyl-methanamines starting from indoles, aldehydes and nitrobenzenes in water. RSC Adv. 2013;3:14308-14311. doi: 10.1039/C3RA41131A

37. Nandhikonda P, Lynt WZ, McCallum MM, et al. Discovery of the first irreversible small molecule inhibitors of the interaction between the vitamin D receptor and coactivators. J Med Chem. 2012;55(10):4640-51. doi: 10.1021/jm300460c

38. Tiwari AP, Sridhar B, Boshoff HI, et al. Design, synthesis, in silico and in vitro evaluation of novel diphenyl ether derivatives as potential antitubercular agents. Mol Divers. 2020;24(4):1265-1279. doi: 10.1007/s11030-019-09990-z

39. Verma R, Boshoff HI, Arora K, et al. Synthesis, antitubercular evaluation, molecular docking and molecular dynamics studies of 4,6-disubstituted 2-oxo-dihydropyridine-3-carbonitriles, J Mol Struct. 2019;1197(2):117–133. doi: 10.1016/j.molstruc.2019.07.035

40. Eum SY, Kong JH, Hong MS, et al. Neutrophils are the predominant infected phagocytic cells in the airways of patients with active pulmonary TB. Chest. 2010 Jan;137(1):122-8. doi: 10.1378/chest.09-0903

41. Wang Q, Boshoff HIM. Determining Minimum Inhibitory Concentrations in Liquid Cultures or on Solid Medium. Methods Mol Biol. 2021;2314:595-609. doi: 10.1007/978-1-0716-1460-0_26

42. D. Alland, A. J. Steyn, T. Weisbrod, K. Aldrich and W. R. Jacobs. Characterization of the Mycobacterium tuberculosis iniBAC Promoter, a Promoter That Responds to Cell Wall Biosynthesis Inhibition. J Bacteriol. 2000.182(7):1802–1811. https://doi.org/10.1128/jb.182.7.1802-1811.2000

43. Naran K, Moosa A, Barry CE, et al. Bioluminescent Reporters for Rapid Mechanism of Action Assessment in Tuberculosis Drug Discovery. Antimicrob Agents Chemother. 2016;60:6748–6757. doi: 10.1128/AAC.01178-16